Mon. Not. R. astr. Soc. (1989) **237**, 381–410

A technique for separating the galactic thermal radio emission from the non-thermal component by means of the associated infrared emission

A. Broadbent,[1] C. G. T. Haslam[2] and J. L. Osborne[1]

[1] *Department of Physics, University of Durham, South Road, Durham DH1 3LE*

[2] *Max-Planck-Institut für Radioastronomie, Auf dem Hügel 69, D-5300 Bonn 1, FRG*

Accepted 1988 September 13. Received 1988 September 13; in original form 1988 August 1

Summary. A detailed correlation is shown to exist between the *IRAS* 60-μm band emission from the galactic disc and the radio continuum emission measured with a similar angular resolution by Reich *et al.* at 11 cm and Haynes *et al.* at 6 cm. A major part of the radio continuum at these frequencies is from thermal bremsstrahlung, and the detailed correlation with the 60-μm band emission shows that an important fraction of the latter must be associated with H II regions (not only the compact regions but also the extended low-density regions). To reveal this component more clearly, the infrared emission from H I-associated dust has been modelled in detail and subtracted from both the 60- and 100-μm band observations. The 60-μm band emission is a sufficiently good tracer of the thermal component of the radio continuum emission that it can be used to separate this from the synchrotron component. This technique is applied first to the identification of new supernova remnant candidates from the Haynes *et al.* survey and secondly to the separation of the emission of the all-sky survey of Haslam *et al.* into its thermal and synchrotron components.

1 Introduction

The problem of distinguishing the thermal and non-thermal components of the radio continuum emission of the Galaxy dates back to the beginnings of radioastronomy. The non-thermal, synchrotron emission dominates at low frequencies while the thermal bremsstrahlung emission becomes prominent at higher frequencies. The standard method of separation requires accurate absolute measurements of the brightness temperature of the continuum emission at high and low frequencies and an *a priori* knowledge of the spectral index of the non-thermal component. We describe here the application of a technique for identifying the thermal component of the radio continuum emission by its associated infrared emission. This component may then be subtracted leaving a clearer picture of the synchrotron emission.

The technique has been outlined in the papers by Haslam & Osborne (1987) (Paper I) and Broadbent, Osborne & Haslam (1988). It is based on the remarkably detailed correlation between the *IRAS* 60-μm band emission from the galactic plane and most of the features seen in the 11-cm radio continuum survey by Reich *et al.* (1984) and the 6-cm survey by Haynes *et al.* (1978), both of which have the same, ~4-arcmin angular resolution as the *IRAS* survey. We illustrated this in Paper I with grey-scale pictures of part of the galactic plane as seen at wavelengths of 60 μm and 11 cm. It can be seen from Plate 1 that the same detailed correlation is apparent when one compares the 60-μm and 6-cm continuum emission. It was known, of course, before the *IRAS* survey was made, that discrete H II regions were sources of radio and infrared continuum emission and that the distribution of far-infrared emission along the galactic plane was similar in form to that of the high-frequency radio continuum. The *IRAS* survey now gives direct evidence through this detailed correlation that an important component of the 60- and 100-μm band emission from the galactic disc is associated not only with discrete H II regions but also with the more extended low-density (ELD) H II regions. We contend that the observations show that the ratio of infrared to radio emission from these regions is sufficiently constant that the residual infrared emission, after allowance has been made for the emission from the H I-associated dust, can be used as a tracer of the thermal component of the radio emission. The procedure for identifying this thermal component is as follows. The zodiacal light contamination is removed from the 60-μm data. The emission from H I-associated dust is modelled and removed. An empirical relation between the residual 60-μm emission and the thermal parts of the 11- and 6-cm emission is found. Finally this empirical relation is used to subtract the thermal component from radio continuum maps pixel by pixel.

It was also noted in Paper I that catalogued supernova remnants which are bright sources on the radio maps show no distinguishable emission on the infrared maps. While discrete H II regions have 60-μm to 11-cm flux density ratios $\geqslant 500$, the corresponding ratios for known supernova remnants are <20. This gives a simple way of finding candidate supernova remnants near the galactic plane. This use of the infrared data has also been proposed independently by Fürst, Reich & Sofue (1987).

The most significant development of the method given in Paper I concerns the treatment of the H I-associated emission. There, relying on an argument of Mezger, Mathis & Panagia (1982) that the interstellar radiation field (ISRF) remains practically constant over the whole Galaxy, we had assumed that the infrared emission per hydrogen atom from the H I-associated dust would also be constant throughout the Galaxy. This meant that the empirical relation between the H I column density and the infrared emission determined at high galactic latitudes, where the H II-associated emission is negligible, would apply down to galactic latitude $b=0°$. Applying this relation to the measured H I column densities in the galactic plane, we found that the contribution of the H I-associated emission was typically <10 per cent of the total infrared intensity in the inner part of the Galaxy and it was therefore not necessary, for the purpose of thermal–non-thermal separation, to consider this component in great detail. The more recent work of Cox, Krügel & Mezger (1986) uses the ISRF as modelled by Mathis, Mezger & Panagia (1983) which increases strongly towards the centre of the Galaxy. The resulting increase in the temperature of the dust grains means that the 60-μm band emission per hydrogen atom is expected to vary by a factor of up to 100 as a function of galactocentric radius. We have recalculated the H I-associated emission for this model. The effect can be seen in Fig. 5. Although the H I-associated emission still does not dominate at $b=0°$, it is no longer a minor contribution. As a consequence we need to give further consideration to the modelling of this emission.

The scheme of this paper is as follows. The components of the infrared emission are discussed in Section 2. The procedures for removal of zodiacal light and the calculation of the H I-associated component are described. This leads to the problem of accounting for the

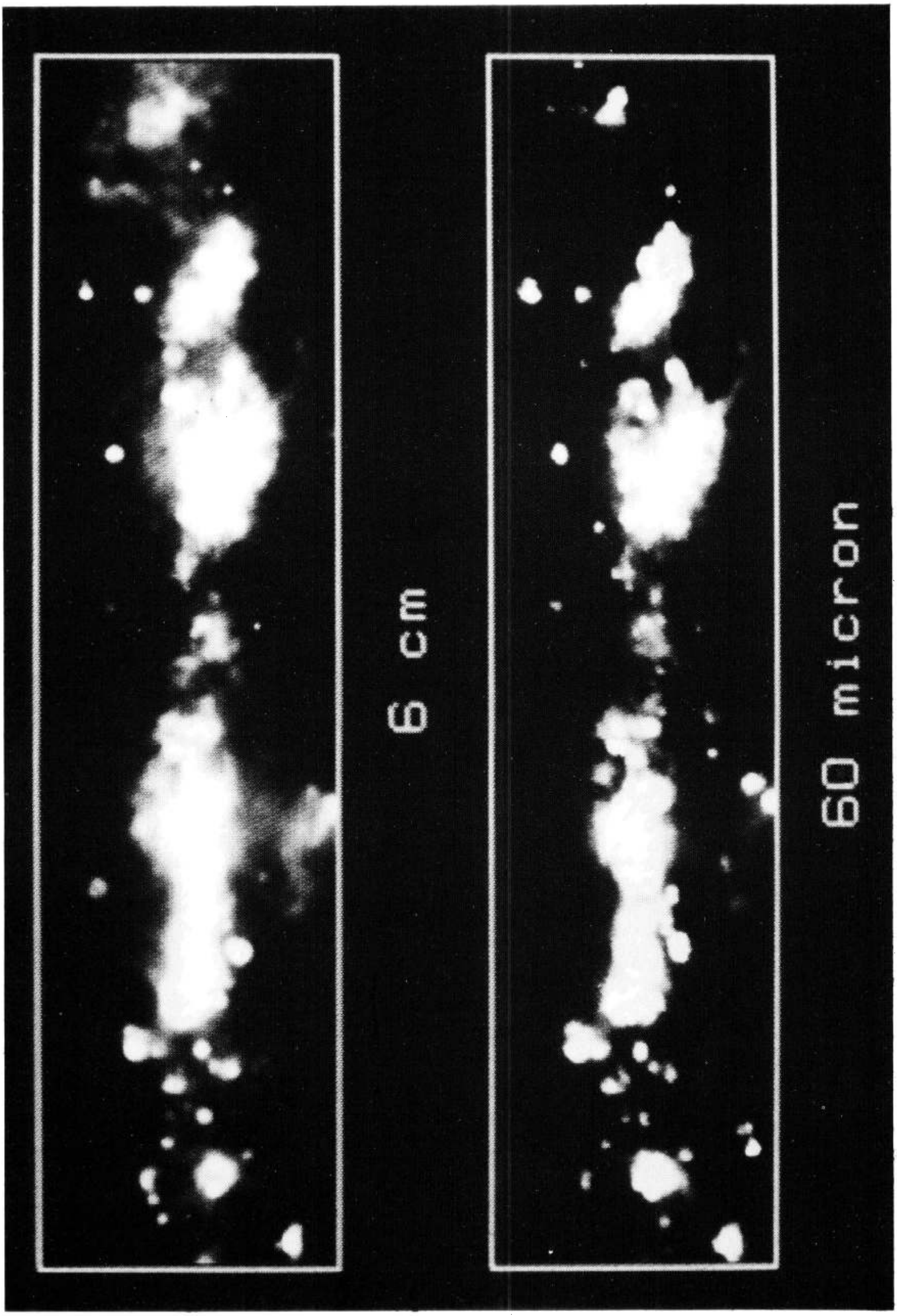

Plate 1. Illustration of the detailed correlation between the *IRAS* 60-μm band emission and the 6-cm radio continuum emission. A section of the galactic plane is shown extending from $l = 341°$ on the right to $l = 329°$ on the left and having $-1°.5 < b < +1°.5$. The upper map shows the 6-cm intensities of Haynes *et al.* (1978). The lower map shows the *IRAS* 60-μm band intensities after removal of the zodiacal light and the modelled H I-associated infrared emission. Note the supernova remnants at $l = 340°.6$, $b = +0°.3$ and $l = 337°.3$, $b = +1°.0$ which appear on the radio map but not on the infrared map. [*facing page* 382]

colour temperature of the infrared emission. It has become apparent that the emission solely from dust grains, whose composition and size distribution is as prescribed by Mathis, Rumpl & Nordsieck (1977), would not have as uniform a colour temperature as is observed. It seems likely that, in addition to these 'standard grains' whose properties were chosen primarily to match the optical and ultraviolet absorption in the interstellar medium, there is a population of 'small grains' which contribute mainly to the 60-μm band emission. It is also possible, as pointed out by Harwit, Houck & Stacey (1986), that infrared line emission gives a contribution sufficient to alter the apparent colour temperatures as measured by the broadband *IRAS* detectors. Since we regard the uncertainty in the H I-associated component as the main source of error in our thermal–non-thermal separation, we have taken two limiting cases to define the error bounds. Thus we consider the 'standard grain' case, where the H I-associated emission at 60 μm is as predicted for standard grains only and the line emission contribution to the 100-μm band is assumed to account for the colour temperature, and the 'small grain' case where an additional contribution to the 60-μm band emission from small grains is invoked. Section 2 concludes with a discussion of whether the residual emission is associated with the ELD and discrete H II regions, or with Giant Molecular Clouds.

In Section 3 we turn to the radio emission and derive an empirical relation between it and the 60-μm H II-associated emission. This leads to a value for the infrared excess for the H II regions. Section 4 presents the results of the thermal–non-thermal separation technique as applied to the all-sky 408-MHz survey by Haslam *et al.* (1982). A list of supernova remnant candidates from the 6-cm survey is given in the Appendix. In the final section, a comparison is made with thermal–non-thermal separation via spectral index analysis.

Although the main aim of the present work is to use the H II-associated emission as a tracer of the thermal radio emission, we do also obtain values for the relative contributions of H I- and H II-associated dust to the 60-μm emission and the mass of ionized gas in the Galaxy.

2 Infrared emission

2.1 *IRAS* DATA

In 1983 the *IRAS* satellite surveyed the infrared sky in four wavebands centred on 12, 25, 60 and 100 μm. Details of the survey are given in the *IRAS Explanatory Supplement* (1985). We have used the galactic plane version of the sky flux plates in the comparison with the radio continuum emission. Specifically, most of the analysis has been performed using the HCON 1 (first hours confirmed) survey. We have used the HCON 2 survey to fill in some blank areas around the anticentre direction. From a comparison of selected areas in both HCON 1 and 2, it appears that any differences between these two surveys are insignificant for the work reported here. The form of the detectors in the focal plane of the infrared telescope, and the method of scanning, results in an effective angular resolution for the surveys of 4–6 arcmin.

We are concerned with the diffuse infrared emission. This consists of zodiacal light from the Solar System, which in the present analysis is a contamination of the data and has to be removed, and the galactic component. There is general agreement that the latter comes from interstellar dust heated by starlight, but there is some debate on the location of the dust grains, whether in H I regions, H II regions or in clouds of molecular hydrogen, and on the sources of the interstellar radiation which contribute most to the heating. One must bear in mind also the possibility of some contribution from infrared line emission which, in the broadband *IRAS* detectors, could not be distinguished from the continuum emission from the dust.

We first consider the removal of the zodiacal light component from the 60- and 100-μm data. We next predict the contribution of the H I-associated dust and remove it. Finally we consider the evidence as to whether the remaining emission correlates with the distribution of molecular gas or with H II regions.

2.2 ZODIACAL LIGHT EMISSION

It is necessary to subtract from the galactic plane survey the contribution from the dust associated with the Solar System. Here, taking note of the observation by Burton *et al.* (1986) that the zodiacal emission variation with ecliptic latitude is very similar all along the ecliptic plane, we have taken the simplest model, where it is regarded as a function of ecliptic latitude only. More complex models (e.g. that of Boulanger & Pérault 1988), in which dependence on such other parameters as solar elongation and time is included, are certainly needed when studying the galactic emission at high galactic latitudes. This zodiacal emission accounts for only a small fraction of the 60- and 100-μm emission near the inner galactic plane on which our study is concentrated, and so an approximate estimate of its intensity is sufficient. The relative importance of the zodiacal emission increases towards the anticentre direction and at high galactic latitudes.

In estimating the 60-μm band zodiacal light emission, it is assumed that at high galactic latitudes ($|b|>20°$) the emission in both 60- and 100-μm bands is dominated by two components, one emanating from dust in the Solar System and the other from dust associated with neutral atomic hydrogen (H I) in the solar neighbourhood. We assume that, for both of these components, the 60- to 100-μm band intensity ratios are constant over this area of sky, and that there exists a linear relationship between infrared emission from the H I-associated dust and the H I column density.

If, in a given direction, I_{60} and I_{100} are the total IR intensities from the 60- and 100-μm bands respectively, I_{ZL} is the intensity at 60 μm of the zodiacal light and N_H is the H I column density then $I_{60}=I_{ZL}+CN_H$ and $I_{100}=AI_{ZL}+CN_H/B$ where A, B and C are constants.

To determine the value of A, the ratio of the 100- to 60-μm band zodiacal light intensities, an all-sky map of H I column densities on a 1° rectangular grid was used. This map had been created using the Berkeley survey (Weaver & Williams 1973) and the Durham–Parkes survey (Strong *et al.* 1982) for the area within 10° of the galactic plane. The data for higher latitudes were from Heiles & Cleary (1979) and Heiles & Habing (1974). For each latitude in the range $40°<|b|<70°$, a pair of points of equal N_H was chosen. One of the pair was near the position of maximum zodiacal light and the other near the minimum. This ensured that the intensity differences at 60 and 100 μm between the two points was as large as possible, minimizing the percentage uncertainty. A value of A for each pair of points was determined using the expression

$$A=[I_{100}(1)-I_{100}(2)]/[I_{60}(1)-I_{60}(2)],$$

where $I_\lambda(1)$, $I_\lambda(2)$ are intensities of the points in the pair at either 100 or 60 μm. Values of I_λ were obtained from all-sky maps binned in a similar manner to the H I column densities and were derived from the HCON 1 low-resolution all-sky maps. There were a few latitudes for which no values could be obtained because of gaps in the survey. The average of all 52 values of A thus derived was 0.37 ± 0.05.

In order to proceed, a value is required for B, the 60–100-μm intensity ratio for H I-associated emission. In Section 2.3, for the 'standard grain' variant of the IR emission of H I-associated dust in the galactic disc, we use the model by Cox *et al.* (1986) in which the cold dust associated with atomic hydrogen has temperatures in the range 15–25 K. With an average dust temperature of 20 K for this dust component in the solar neighbourhood, and the grains following an inverse-square wavelength emissivity law over the 60- and 100-μm bands, the 60–100-μm intensity ratio, B, is approximately 0.1.

Using these values of A and B, the value of C, the 60-μm intensity to H I column density ratio, can be calculated for every point on the rectangular grid with $|b| > 20°$. An average of all these values was found to be 0.14 MJy sr^{-1} $(10^{20}\ cm^{-2})^{-1}$. Using this, the emission due to H I-associated dust can be subtracted from the $|b| > 20°$ part of the 60-μm all-sky map. The residual 60-μm all-sky map was transformed to ecliptic coordinates and an average profile along the ecliptic was obtained, avoiding the area with $|b| < 20°$ and removing spikes caused by the Large Magellanic Cloud and the Orion Nebula. This profile, shown as the dashed line in Fig. 1, was used to map the 60-μm zodiacal emission which was then subtracted from the 60-μm band *IRAS* HCON 1 galactic plane survey. In subtracting the zodiacal light contamination in this way, we will also eliminate any isotropic component such as an extragalactic background.

In Fig. 2, the cross-cut at $l = 10°$ illustrates that the zodiacal light contamination in the 60-μm band is only a small contribution to the total emission along the galactic plane in the inner part of the Galaxy (~ 3 per cent at $l = 10°$, $b = 0°$) and justifies the use of such an approximate method of removal here. Obviously, as shown by the cross-cut at $l = 240°$, in the outer plane the zodiacal emission is a substantial fraction of the total 60-μm intensity (~ 90 per cent at $l = 240°$, $b = 0°$) and errors in the estimation of this contribution are more important.

These results are based on the predicted value, $B = 0.1$, obtained using the grain size distribution from Mathis *et al.* (1977), which we have referred to as the 'standard grain' results. Studies of the intensities in the 60- and 100-μm bands at high galactic latitudes by Terebey & Fich (1986), Boulanger & Pérault (1988) and Low *et al.* (1984) show the observed ratio to be closer to $B = 0.2$. As discussed further in Section 2.3, an explanation of this involves an

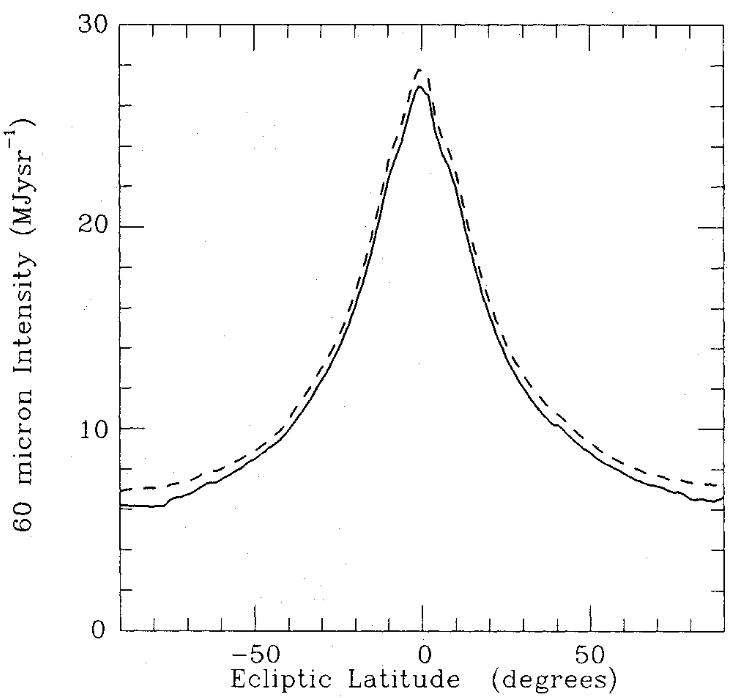

Figure 1. The variation of zodiacal light intensity at 60 μm with ecliptic latitude. This is the mean variation averaged over all ecliptic longitudes. As a first-order approximation, sufficiently accurate when working close to the galactic plane, the same variation has been used at all ecliptic longitudes. The two curves show the sensitivity to the assumed ratio of 60–100-μm intensities for galactic emission at high galactic latitudes. The ratio is 0.1 for the dashed line ('standard grains') and 0.2 for the solid line ('small grains').

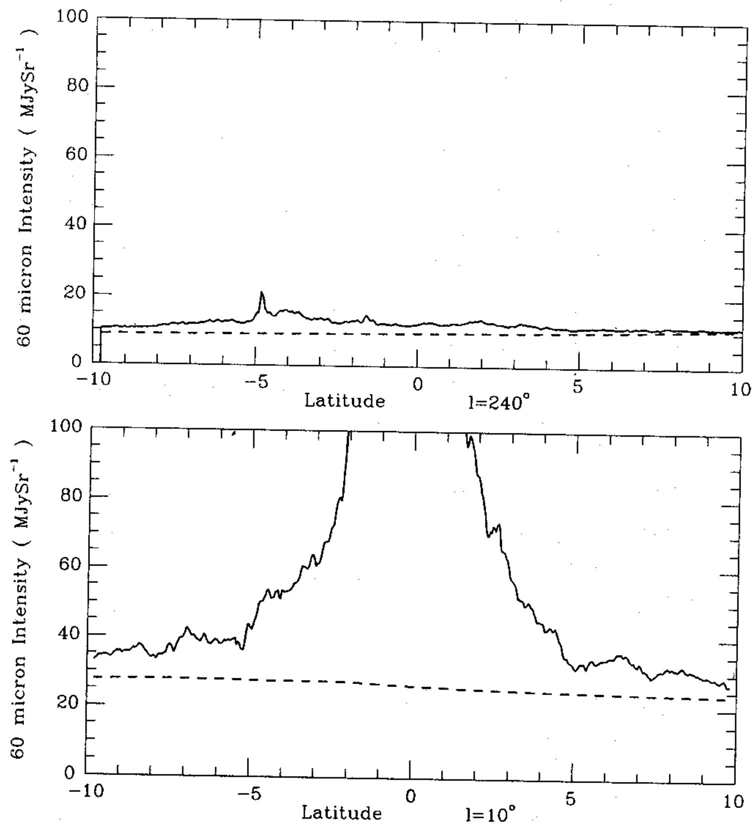

Figure 2. Cuts across the galactic plane showing the total observed 60-μm intensities (solid lines) and the modelled zodiacal light for the 'standard grain' variant (dashed lines). The lower plot at $l=10°$ has the zodiacal light close to its maximum value. It is a minor component, however, within a few degrees of the galactic plane (the peak value of the total emission is 1011 MJy sr^{-1}). The upper plot at $l=240°$ shows that part of the plane where the total emission is at a minimum and the zodiacal light has its greatest relative contribution.

additional population of very small grains. If we repeat the above procedure with this value of B, the value of C, the mean intensity at 60 μm per unit column density of atomic hydrogen, becomes 0.285 MJy sr^{-1} (10^{20} cm^{-2})$^{-1}$. [We note that the corresponding ratio at 100 μm, 1.4 MJy sr^{-1} (10^{20} cm^{-2})$^{-1}$, is insensitive to the value of B.] This in turn gives a second average profile of zodiacal emission across the ecliptic plane, which is shown as the solid line in Fig. 1. It can be seen that the two profiles differ by only a few tenths of a MJy sr^{-1}. This difference is negligible when studying the region close to the galactic plane but could be significant when comparing the models of H I-associated emission with the total galactic emission at higher latitudes.

2.3 Emission from H I regions

In modelling the IR emission from H I-associated dust, we have to take into account the variation of emissivity of dust grains per hydrogen atom with galactocentric radius and the three-dimensional distribution of H I in the galactic disc. The velocity information of the Berkeley and Durham–Parkes surveys was used with the galactic rotation curve of Burton & Gordon (1978) to determine the distribution of H I with galactocentric radius along a given line of sight. Hence the intensity of infrared emission from H I-associated dust in that direction could be calculated by using the predicted emissivity per H atom for the appropriate *IRAS* band. This prediction depends on the dust grain model used. First we show the results of the 'standard grain' model, then we discuss the problem of matching the observed colour temperature of the radiation and finally we consider the results of the alternative 'small grain' model.

2.3.1 *The 'standard grain' model*

This was derived using the predictions of Cox *et al.* (1986) for the variation with galactocentric radius of absorption cross-section per H atom and temperature of dust grains. We note that the temperature variation of the dust grains, dictated by the interstellar radiation field, is the major factor causing a steep rise in the emissivity per H atom, towards the Galactic Centre. The variation of absorption cross-section per H atom, which is assumed to follow the metallicity gradient (Güsten & Mezger 1983), has a much smaller effect. The model of the dust grains used by Cox *et al.* is that of Mathis *et al.* (1977) modified by Draine & Lee (1984), and assumes a mixture of silicate and graphite grains of size distribution $f(a) \propto a^{3.5}$ where a is the grain radius. In a comparison with *IRAS* data, it is necessary to include a small correction in the predictions to take into account variation of emissivity of the dust grains and relative system response over the *IRAS* passbands.

We used this method to model the 60-μm intensity of the H I-associated dust for the whole of the galactic plane for $|b| < 10°$, except for the Galactic Centre and anticentre directions. Within a few degrees of these directions, the assumption of circular rotation in obtaining the distance of the emitting H I regions breaks down, and towards the Galactic Centre the H I emission is optically thick. In the anticentre direction one can interpolate the H I-associated dust contribution with sufficient accuracy. We recognize that in the Sgr A source direction, however, we may not have correctly estimated this emission. It may well be that the relationship between the 60-μm band emission and the thermal radio emission which we derive empirically in Section 3.2 for the rest of the Galaxy cannot be applied to the special conditions in the Sgr A source region. We do not therefore claim that our thermal–non-thermal separation technique necessarily applies to this particular region.

We note that both the Berkeley survey and the Durham–Parkes survey are at lower resolution, 35.5 and 15 arcmin respectively, than the 4 arcmin of the *IRAS* galactic plane survey. In addition, the Durham–Parkes survey is undersampled. We have not convolved the *IRAS* data to these lower resolutions before subtracting the H I-associated emission, as we would thereby lose important information on the detailed correlation between the infrared and radio continuum emission. In the region $|b| < 1\overset{\circ}{.}5$, where we study this correlation, the H I-associated emission is a minor component, and the fact that our estimate of it is based on lower-resolution data simply adds noise to the correlation.

Fig. 3 shows the profile, averaged over $|b| < 0\overset{\circ}{.}5$ for the inner galactic plane, of the 60-μm band intensity with the zodiacal light contamination removed, together with the corresponding profile for the predicted H I-associated dust intensity. The averaging should help to reduce the discrepancies introduced because of the different resolutions of the H I and *IRAS* surveys.

Fig. 4 shows six typical cuts across the galactic plane taken at longitudes in all four quadrants. Again, the *IRAS* 60-μm intensity with zodiacal light removed is shown, together with the predicted contribution from H I-associated dust. It can be seen that, at the higher latitudes, where we would expect there to be little ionized hydrogen, the two curves converge remarkably well, considering that at these latitudes the estimated zodiacal light contamination is several times larger than the residual galactic emission. This can be seen by comparing the cuts for $l = 240°$ in Figs 2 and 4. It should be emphasized that these latitude distributions of H I-associated 60-μm emission differ from the distributions of H I column density at corresponding longitudes. In the inner half of the galactic plane the predicted distributions are more strongly peaked than the H I column density distributions. This means that it is not safe simply

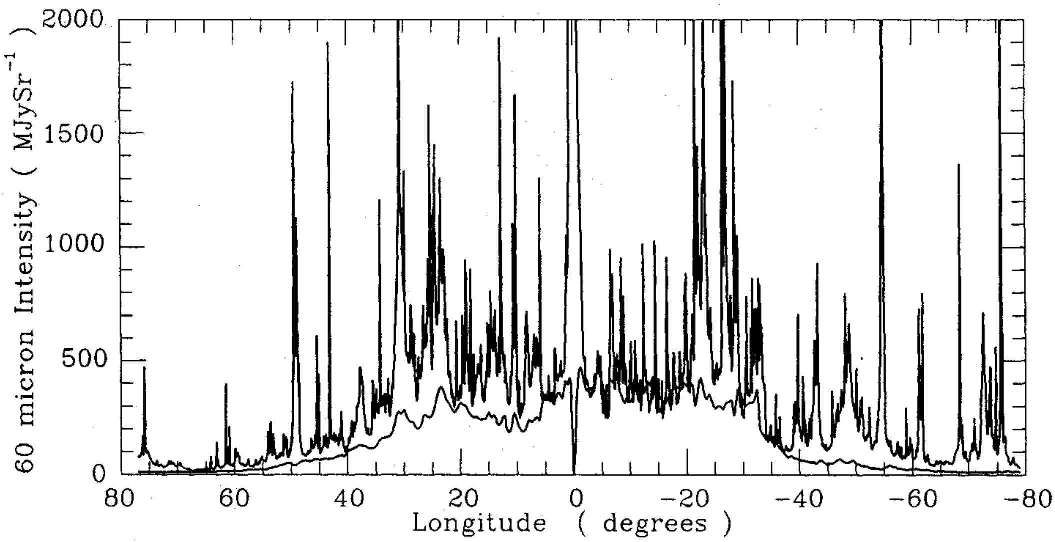

Figure 3. Profiles of the total observed 60-μm band emission for the inner part of the galactic plane averaged over $-0^\circ\!.5 < b < +0^\circ\!.5$ and the modelled component from H I-associated dust (lower curve). (The local minimum at $l = 0°$ is an artefact of the modelling.)

to decompose the observed infrared emission into H I-, H II- and H_2-associated components using the relative scale heights of the corresponding components of the interstellar gas.

2.3.2 *The colour temperature of the infrared emission*

We applied the same procedure to modelling the emission in the 100-μm band for part of the first quadrant ($79^\circ\!.5 \geq l \geq 10°$) within 10° of the galactic plane. Fig. 5 shows profiles for the 60- and 100-μm bands for $53° \geq l \geq 13°$. Each line represents an average over $\pm 0^\circ\!.5$ of latitude. The higher profile in each plot is the infrared emission after removal of the zodiacal light contamination. The lower solid line is the predicted H I-associated dust contribution. For the 60-μm band the dotted line is the predicted H I-associated dust contribution had we assumed that the ratio of 60-μm emission to hydrogen column density was constant for the whole of the galactic plane, with the solar neighbourhood value of 0.14 MJy sr^{-1} (10^{20} cm^{-2})$^{-1}$ (see Section 2.2).

Over the area for which both the 60- and 100-μm band H I-associated dust contributions have been predicted, the *IRAS* galactic plane maps, with zodiacal emission subtracted, have been convolved to the 35.5 arcmin resolution of the 21-cm Berkeley survey. The ratio of the 60- to 100-μm intensities could then be found for (i) the total emission less zodiacal light, (ii) the predicted H I-associated dust emission, and (iii) the residual emission after (ii) has been subtracted from (i). We argue in Section 2.4 that this residual emission is predominantly from H II regions. Profiles of the ratios of intensity, averaged over $\pm 1°$ in galactic latitude for each of these three cases are shown in Fig. 5. The colour temperature corresponding to these *IRAS* intensity ratios, assuming an emissivity of the dust grains which varies as the inverse square of the wavelength, are also marked.

As has been remarked upon by other authors (e.g. Sodroski *et al.* 1987), the colour temperature of the total emission appears to be fairly constant at about 23 K, independent of galactic longitude. The peaks in the profile can be identified with large H II complexes by referring to the 11-cm survey. According to the 'standard grain' model, with which we have been dealing so far, the temperature of the H I-associated dust component increases monotonically with

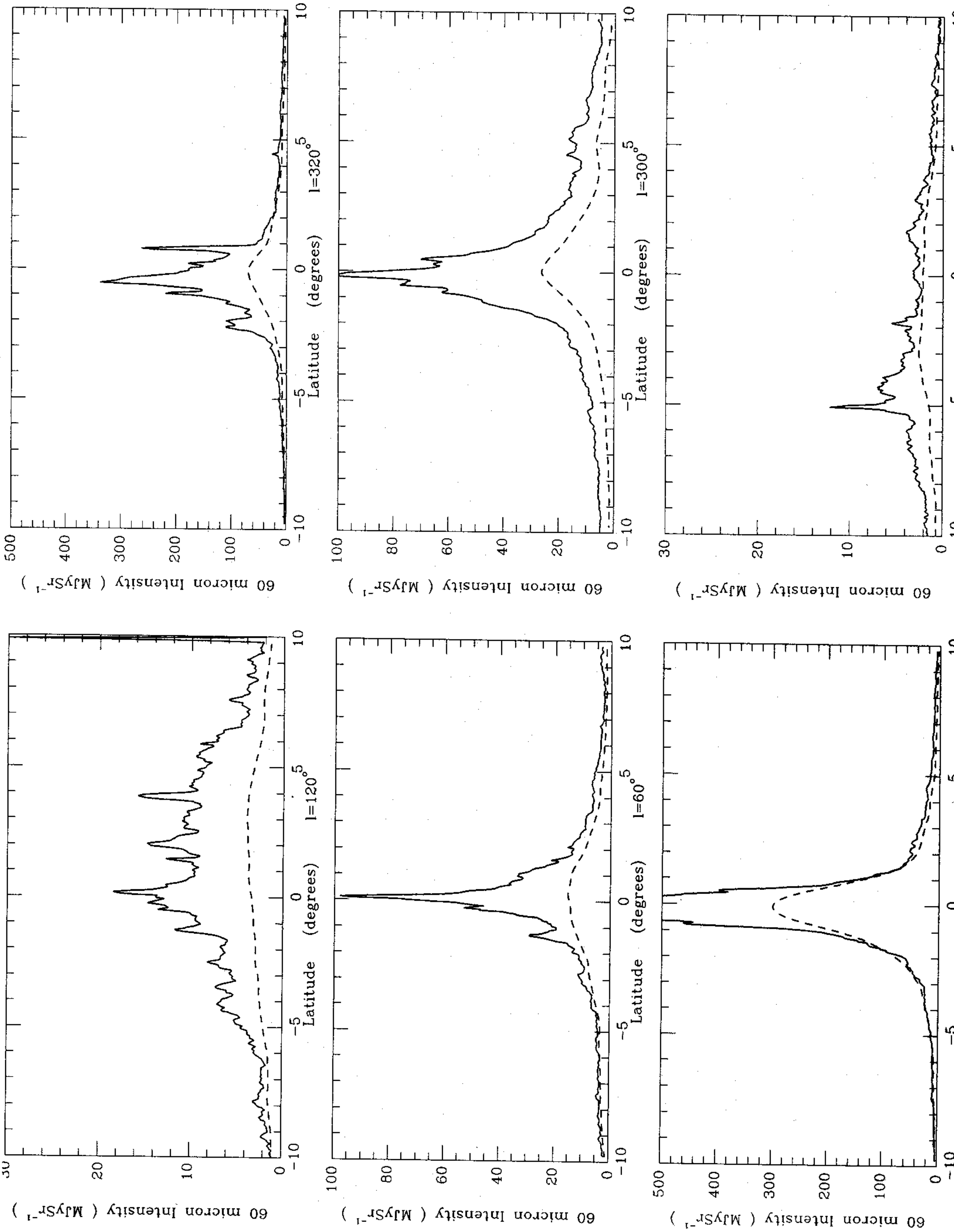

Figure 4. Six cuts across the galactic plane showing the predicted H I-associated component (dashed lines) relative to the total emission. This component fits the observations well at latitudes greater than about 3° for all longitudes except $280° < l < 300°$. It may be that the interstellar radiation field in the Carina arm is higher than given by the assumed purely radial dependence.

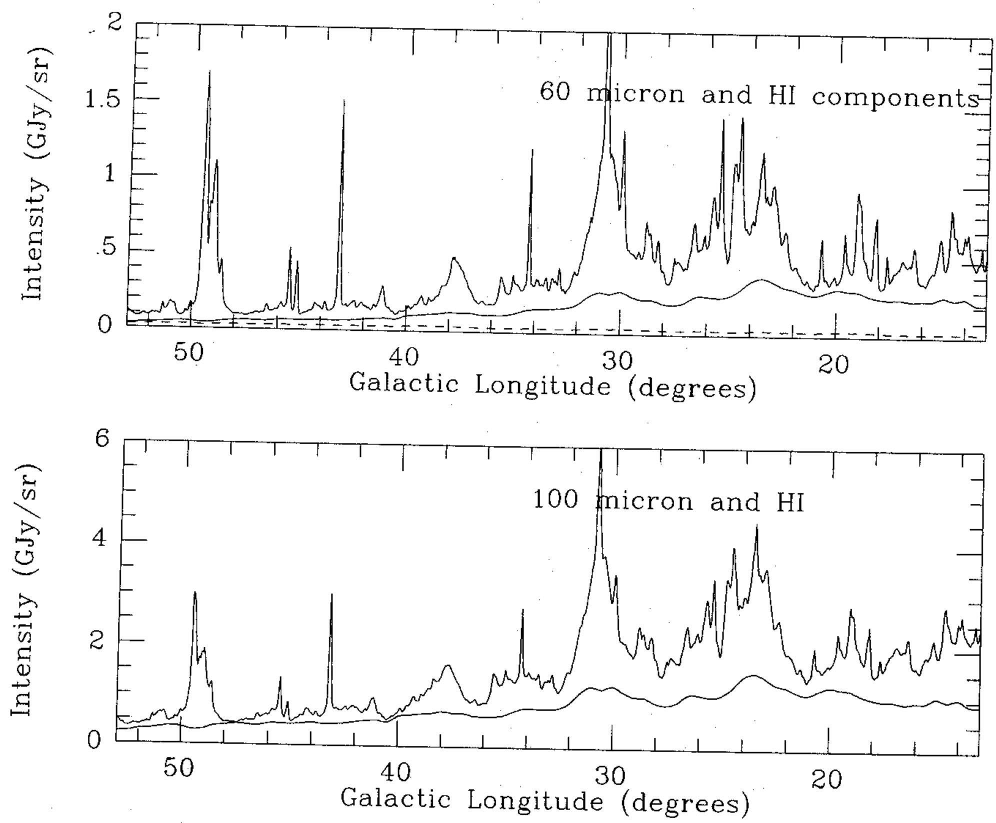

Figure 5. Profiles of 60- and 100-μm *IRAS* intensities along the galactic plane averaged over $-0^\circ.5 < b < +0^\circ.5$. The lower solid lines show the predicted contributions from H I-associated dust, whose variation in temperature with galactocentric radius follows the model of Cox *et al.* (1986). The lower dashed line on the upper plot shows the H I contribution if the dust was all at the temperature appropriate to the solar neighbourhood.

decreasing galactic longitude from a value of about 18 K at $l = 79^\circ.5$ to 24 K at $l = 10^\circ$. This reflects the 17–25 K temperature variation with galactocentric distance of the graphite grains which dominate the emission at 60 and 100 μm in this model (see Section 2.2).

Because of the observed near-constancy of the ratio of 60–100-μm total intensities and the predicted increase towards lower longitudes for the H I-associated component, the implied ratio for the H II-associated component must necessarily decrease towards lower longitudes, as is illustrated in the third profile of Fig. 6. The colour temperature remains fairly constant at ~ 28 K between $l = 79^\circ.5$ and 40° but then drops to ~ 23 K by $l = 10^\circ$.

There are two ways to account for this behaviour. Either there is an additional component in the 100-μm H II-associated emission which causes its colour temperature to be lower than expected or there is an additional component in the 60-μm H I-associated emission which causes its colour temperature to be higher than the 'standard grain' model predicts. We consider these in turn.

Harwit *et al.* (1986) suggested that some of the *IRAS* 100-μm band emission from ionized regions may be due to the emission line of O III at 88.35 μm. There would be no appreciable effect on the 60-μm band intensity so that the apparent temperature of the emission, based on the 60–100-μm ratio would be reduced. For the effect to become larger towards the centre of the Galaxy there would have to be an increase in the $[O^{2+}/O]$ abundance ratio towards the Galactic Centre. The arguments of Terebey & Fich (1986) against a significant contribution from line emission are based upon observations of regions in the outer parts of the Galaxy. They do not rule out a contribution in regions of higher radiation density in the inner Galaxy.

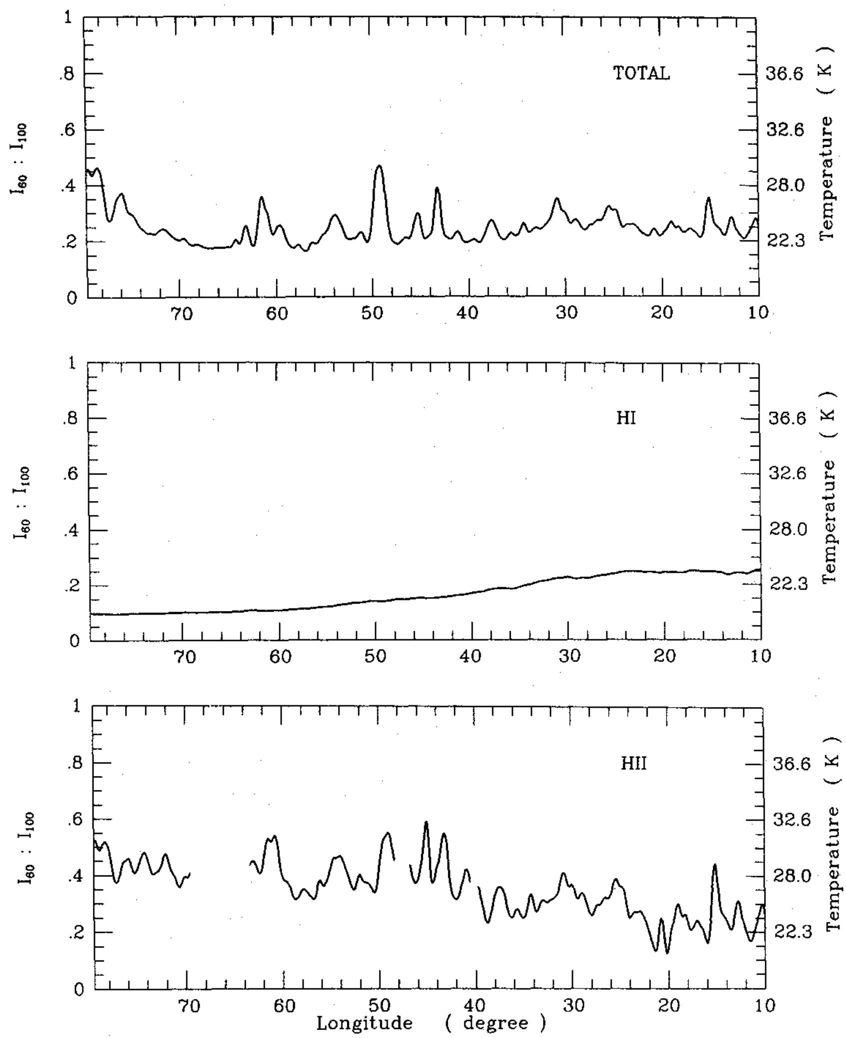

Figure 6. Profiles of the ratio of 60–100-μm intensity along the galactic plane. The top curve shows the observed values. The middle curve is the predicted ratio for the H I-associated emission. The bottom curve shows the ratio of the residuals when the H I-associated emission has been subtracted from the observed values. Blank regions appear where the residual 100-μm emission is very small and the error in the ratio would be very large. The implied colour temperatures are shown on the right-hand side.

Present measurements of the O III line give no conclusive test of this hypothesis. A necessarily rough estimate for M17 using the line measurements by Watson *et al.* (1981) suggests that, for this H II region, the contribution to the 100-μm band *IRAS* flux from the 88-μm line might be about 6 per cent. Attempts to establish the behaviour of [O^{2+}/O] with galactocentric radius have been thwarted by a lack of data for H II regions within 6 kpc of the Galactic Centre. If this line emission did account for the apparent colour temperature of the galactic plane emission, it would be appropriate to use the 'standard grain' model for the subtraction of the H I-associated component in the 60-μm band.

An alternative explanation of the uniform colour temperature of the total emission was put forward by Draine & Anderson (1985) who invoked a population of very small particles in addition to the Mathis, Rumpl & Nordsieck (1977) grain distribution in order to explain the uniform colour temperature of the emission. Large temperature variations are expected for these small particles due to heating by a single UV photon from the general ISRF. Calculations by Draine & Anderson of the expected emission spectra show that the emission from these very small grains would contribute little to the 100-μm intensity but would make a significant contribution to the 60-μm band. We need to consider the effect of this 'small grain' model as it increases the H I-associated component to be subtracted from the total 60-μm emission when obtaining the residual, H II-associated, emission.

2.3.3 *The 'small grain' model*

To investigate the 'small grain' model in detail, one would have to model the emission of the various species of small grains in the ISRF which is varying with galactocentric radius. However, bearing in mind that the properties of these grains have mainly been chosen in order to give a constant colour temperature of the H I-associated emission, we can easily estimate the magnitude of the effect. We use our predictions of the H I-associated emission in the 100-μm band described in the previous sections scaled by a factor of 0.2 to model the 60-μm band emission. We choose the constant factor of 0.2 by consideration of Fig. 6 and the higher galactic latitude results referred to in Section 2.2.

Fig. 7 shows examples of two cuts across the galactic plane. The solid line represents the observed 60-μm band emission with the appropriate 'small grain' solution for the zodiacal emission subtracted, and the dashed line is the predicted 100-μm band H I-associated emission scaled by 0.2. These two profiles can be compared with the corresponding ones in Fig. 4. In general, the new estimate of the H I-associated emission is a fairly good fit in the

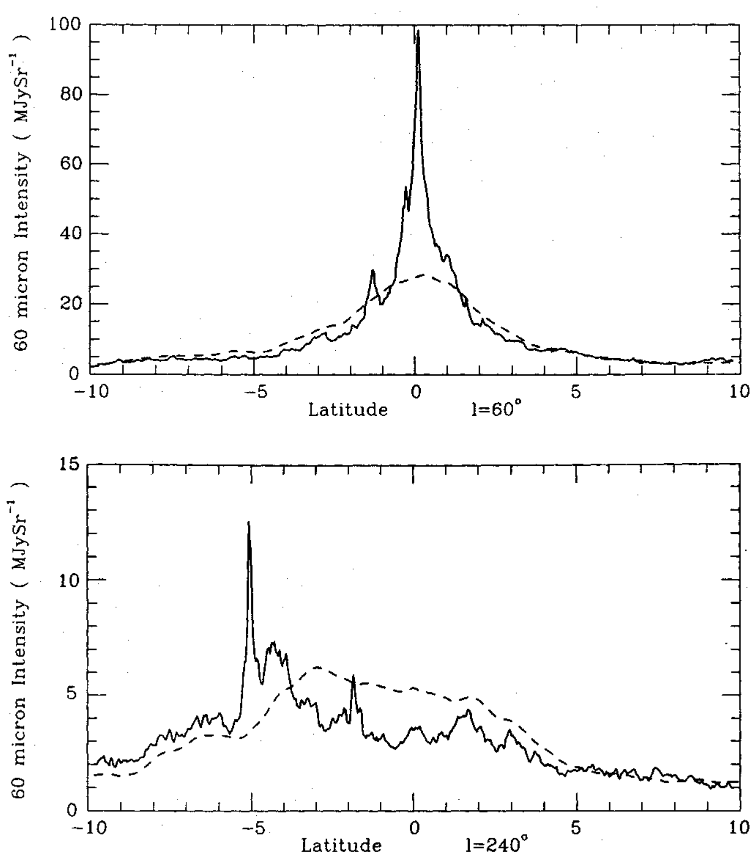

Figure 7. Two cuts across the galactic plane showing the predicted H I-associated component for the 'small grain' variant (dashed lines) relative to the total emission. These are to be compared with Fig. 4 which shows the 'standard grain' variant.

wings ($|b| \geqslant 5°$) but tends to be higher than the observed total emission at intermediate latitudes ($2° \leqslant |b| \leqslant 5°$).

2.4 EMISSION FROM MOLECULAR CLOUDS

Before one accepts from the qualitative evidence of Plate 1 that the residual 60-μm emission is from H II-associated dust, one should consider the possibility that it comes from dust in molecular clouds. It is clear that, if the dust in the clouds were heated by the general ISRF attenuated by absorption, its temperature would not be high enough to give any significant contribution to the 60-μm flux. It is possible, however, that the dust is heated by embedded, and thus unobservable, O and B stars.

We have used data from the Massachusetts–Stony Brook ^{12}CO survey (Sanders *et al.* 1986) to give the profile of velocity-integrated CO emission shown in Fig. 8(c). The survey has a sampling interval of 3 arcmin but it is considerably undersampled as the beam size is 45 arcsec. Unfortunately there is at present no fully sampled survey covering an appreciable area of the galactic plane. Strips in galactic longitude observed with more closely spaced points have enabled the distribution of molecular cloud sizes to be determined. The authors of the present survey conclude that their point spacing of 3 arcmin is small enough to resolve clouds containing 85 per cent of the total molecular gas. Our averaging over $|b| < 0.°5$ to some extent

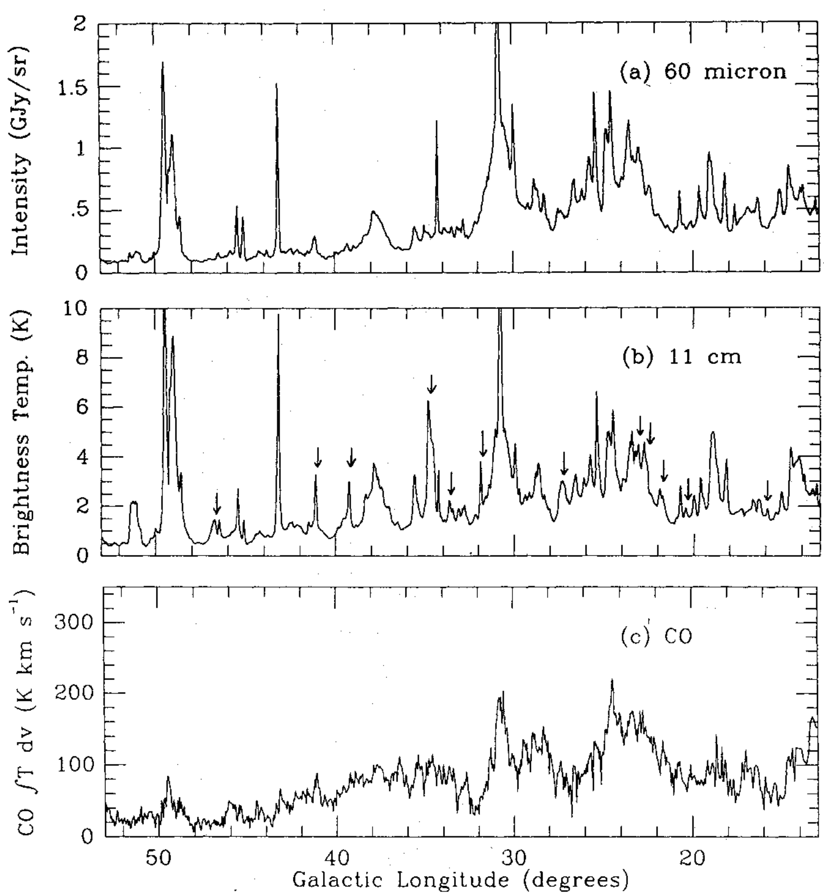

Figure 8. Comparison of profiles along the galactic plane of (a) the 60-μm band *IRAS* emission after subtraction of the modelled H I-associated component, (b) the 11-cm radio continuum emission from Reich *et al.* (1984), with peaks due to known SNR marked by arrows, (c) ^{12}CO column densities from the Massachusetts–Stony Brook survey. All are averaged over $-0.°5 < b < +0.°5$.

compensates also. In principle, the intensity of the CO line emission should vary in proportion to the column density of H_2 only if the clouds are optically thin. This is not the case for ^{12}CO but, in practice, there is a close resemblance between sample spectra observed in the same direction in ^{12}CO and in the optically thin ^{13}CO line, with the latter having a five times lower intensity. It seems then that the CO profile represents also the variation with galactic longitude of the column density of molecular hydrogen. The similarly averaged profile of 11-cm radio continuum is shown in Fig. 8(b) and the profile of 60-μm infrared emission, after the removal of the zodiacal light and the H I-associated emission, is shown in Fig. 8(a). It is clear that there is a much tighter correlation between the infrared and the radio continuum than between the infrared and the CO data. There are indeed broad peaks at $l=24°$ and $l=31°$ in all three profiles, but there is a one-to-one correspondence between practically all of the features in the radio and infrared that is not at all apparent between the CO and the infrared. The only 11-cm features which are missing from the infrared are the peaks, marked by arrows, which are due to emission from catalogued supernova remnants.

A quantitative test of the relative correlation is shown in Fig. 9, where scatter plots are given for the region $35° > l > 29°$, $|b| < 1.^{\circ}5$. The CO versus 60 μm correlation coefficient is 56 per cent compared with 82 per cent for the 11 cm versus 60 μm plot. The latter has been reduced by the points close to the vertical axis due to the bright SNR W44. If this is omitted, the correlation exceeds 90 per cent. The degree of correlation which is seen between the CO and 60 μm can be accounted for by the fact that there is general spatial correlation between giant molecular clouds and giant H II regions due to their common association with star formation.

2.5 EMISSION FROM H II REGIONS

The residual infrared emission which correlates strongly with the thermal radio emission appears to be that which comes from the 'warm' dust component in the model by Cox *et al.* (1986). This dust is mainly associated with the gas in ELD H II regions which has been ionized by observable O stars. The diameters of the regions range from 20 to 250 pc and the electron densities are typically 5–10 electrons cm^{-3}.

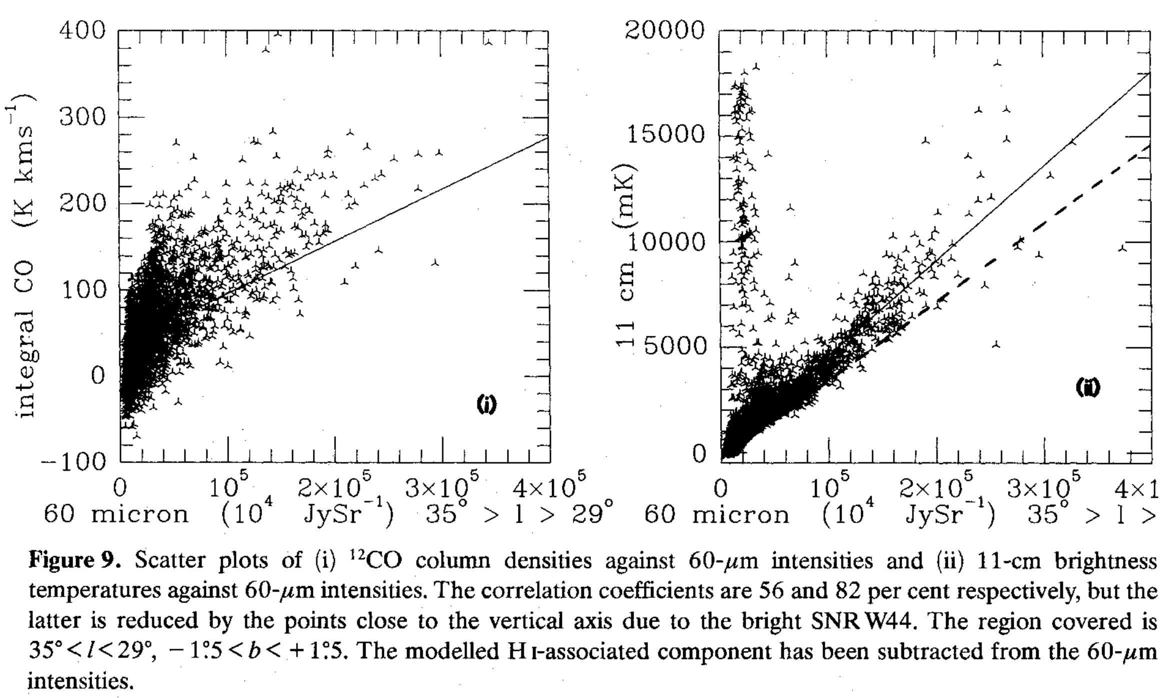

Figure 9. Scatter plots of (i) ^{12}CO column densities against 60-μm intensities and (ii) 11-cm brightness temperatures against 60-μm intensities. The correlation coefficients are 56 and 82 per cent respectively, but the latter is reduced by the points close to the vertical axis due to the bright SNR W44. The region covered is $35° < l < 29°$, $-1.^{\circ}5 < b < +1.^{\circ}5$. The modelled H I-associated component has been subtracted from the 60-μm intensities.

The radio and infrared emissivities of these H II regions are related through the ionization and recombination rate of their atoms. The radio continuum emissivity is proportional to the recombination rate, r. For an H II region which is optically thin at a frequency ν, the emissivity is:

$$\varepsilon_\nu(\text{radio}) = 2\times10^{-36}\, T_e^{0.45}\, \nu^{-0.1} r \quad \text{W cm}^{-3}\,\text{Hz}^{-1}\,\text{sr}^{-1},$$

where T_e is the electron temperature. The weak dependence on frequency is an approximation to the frequency variation of the Gaunt factor. The summed surface brightness of the H II region is also proportional to $\nu^{-0.1}$ and the brightness temperature therefore has a spectral index of 2.1.

Most of the Lyman continuum photons involved in the ionization are eventually degraded into Lα photons which will be absorbed by the dust grains in the H II region, and their energy will be reradiated in the infrared. This emissivity is enhanced by photons of longer and shorter wavelength than the Lα. The enhancement factor, f, is the infrared excess (IRE). The infrared emissivity is thus:

$$\varepsilon(\text{IR}) = frh\nu_\alpha/(4\pi) = 1.3\times10^{-19} fr \quad \text{W cm}^{-3}\,\text{sr}^{-1}.$$

Using the appropriate emissivity law and grain temperature, the emissivity per unit frequency at 60 μm is:

$$\varepsilon_\nu(60\ \mu\text{m}) = 1.9\times10^{-32} fr \quad \text{W cm}^{-3}\,\text{Hz}^{-1}\,\text{sr}^{-1}.$$

With $T_e = 7000$ K the ratio of emissivities at 60 μm and 11 cm is:

$$\varepsilon_\nu(60\ \mu\text{m})/\varepsilon_\nu(11\ \text{cm}) = 190 f.$$

If the radio and infrared emitting regions coincide, the ratio of the intensities of emission will be the same as the ratios of emissivity. Thus the intensity ratio which is obtained in Section 3 leads to a value for the IRE of the ELD H II regions.

3 Radio continuum emission

3.1 THE RADIO SURVEYS

There are two radio continuum surveys with resolution close to that of the *IRAS* sky flux plates which between them cover most of the inner half of the galactic plane. These are the 11-cm survey by Reich *et al.* (1984) and the 6-cm survey by Haynes *et al.* (1978).

The 11-cm survey was made using the Effelsberg 100-m telescope and has a beam size of 4.3 arcmin. The presently published part of the survey covers the area $357.^\circ4 \leqslant l \leqslant 76^\circ$, $|b| \leqslant 1.^\circ5$. Scans were made in galactic latitude over a range of $\pm 1.^\circ5$ except where there are obvious sources at the boundary, in which case more extended scans were made. The survey has its zero level set at $|b| \approx 1.^\circ5$ except in the source-affected regions. The survey will eventually be calibrated to an absolute temperature scale following extension of the scanned region to $|b| = 5^\circ$. This will use a lower resolution survey made with the Stockert 25-m telescope covering the range $|b| < 20^\circ$. An estimate of absolute temperatures can be obtained by noting the temperatures at $|b| = 1.^\circ5$ on the Altenhoff *et al.* (1970) 11-cm survey for longitudes where the zero level of the Effelsberg survey is at $|b| \approx 1.^\circ5$. This gives a profile that varies from 0.5 K at $l \simeq 65^\circ$ to 1.5 K at $l \simeq 0^\circ$. The zero level of the Altenhoff survey was itself set at $|b| = 5^\circ$. From the 408-MHz survey by Haslam *et al.* (1982) and the assumption of a spectral index of 2.8 at this latitude, it seems that a further 0.2–0.6 K should be added to the 11-cm survey to obtain absolute temperatures (excluding the 2.7 K microwave background). Reference to Fig. 8(b) shows that such an addition of 0.7–2.1 K is very significant in terms of the absolute level of the survey and would have to be precisely determined if a thermal–non-thermal separation were to be attempted based on spectral information only. Our method of fitting a lower envelope to a scatter plot of radio against IR intensities is not sensitive to a smoothly varying background provided that each fit covers a restricted range of longitude.

The 6-cm survey was made with the Parkes 64-m telescope and has a beam size of 4.1 arcmin. The continuous part of it covers the range of longitude from $l = 280°$ through the galactic centre to $l = 40°$. Its zero level was set at the ends of its scans which extend to $|b| \simeq 2.5°$. The digitized version that we worked with has a constant offset added. By looking at the temperatures in the wings of a number of cross-cuts over the whole range, we deduced that this constant was 1 ± 0.1 K. An extrapolation of the 408-MHz data at $|b| = 2.5°$ indicates that the absolute temperature at these latitudes is of the order of 0.1 K. Subtraction of 1 K from the digitized values thus gives a best estimate of the absolute temperatures.

3.2 CORRELATION OF RADIO CONTINUUM WITH 60-μm *IRAS* EMISSION

After removal of the zodiacal light and the modelled H I-associated IR emission from the sky flux plates of the galactic plane in the 60-μm band, the next step is to investigate the correlation between the radio continuum emission and the remaining IR emission, with the aim of obtaining a numerical relationship between the IR and the thermal part of the radio emission. This is done by plotting the net IR intensity against the radio brightness temperature pixel by pixel for $|b| < 1.5°$ (pixel size is 2.5×2.5 arcmin^2). Because of the variation with longitude of the absolute base level of the 11-cm survey, a separate plot was made for each 6° interval of galactic longitude. The scatter plots, such as that illustrated in Fig. 9(ii), have well-defined lower envelopes to which straight lines can be fitted. Our interpretation of this is that the net IR emission always has associated thermal radio emission (except for that from stars, which can be identified by their showing maximum brightness in the 12-μm band), and that points on the lower envelope are for directions where the non-thermal emission, above a constant background level for that interval of longitude, is negligible.

Determination of this line objectively is quite difficult. The method adopted here is as follows. Initially, a line is drawn by eye which seems the best representation of the lower envelope. Next a search is made by computer over a range of slopes and y-intercepts about the values estimated by eye. For each line, the number of points which have radio brightness temperature within 100 mK above the value on the line at the same infrared intensity is counted. Similarly, the number of points within 100 mK below the line is determined. If a line exists, away from the edges of the ranges of intercepts and slopes searched, which has the maximum difference in number of points lying within 100 mK above and below the line, then this line is taken to be the lower envelope. An additional constraint is imposed that the number of points lying within 100 mK below the line must be less than 100. (There are 10 000 points on each plot.)

If $y = A_0 x + B_0$ is the equation of the initial line estimated by eye, then the range and increments in slope and y-intercept are:

$$(A_0 - 12 \times 10^{-7}) < A < (A_0 + 12 \times 10^{-7}) \text{ mK Jy}^{-1} \text{ sr}^{-1}$$

$$dA = 2 \times 10^{-7} \text{ mK Jy}^{-1} \text{ sr}^{-1}$$

$$(B_0 - 1000) < B < (B_0 + 1000) \text{ mK}$$

$$dB = 50 \text{ mK}.$$

Although this approach may seem rather arbitrary, it is more systematic and less subjective than an estimation by eye. Fig. 9(ii) shows the plot of 11-cm brightness temperature against 60-μm residual intensity for $35° > l > 29°$, $|b| < 1.5°$. The lower envelope, determined by the above method, is marked. The same procedure has been carried out for the rest of the 11- and 6-cm surveys by dividing the data into areas 6° wide in galactic longitude and extending $\pm 1.5°$ in galactic latitude. Out of all 33 such areas over the two surveys, there were four for which it was not possible to determine a lower envelope by the above method unless points having slightly negative residual intensities were ignored. Such points would be due to over-estimation of the zodiacal light or H I-associated dust emission in particular directions. At 6 cm, for the area including the Galactic Centre, the lower envelope fitting-procedure failed completely and only an estimation by eye could be made.

The average slope from the 13 plots of 11-cm brightness temperature against residual 60-μm intensity is $(6.4 \pm 1.7) \times 10^{-6}$ mK Jy^{-1} sr^{-1} and, for the 20 plots of 6-cm brightness temperature against 60-μm intensity, the average slope and intercept are $(1.6 \pm 0.5) \times 10^{-6}$ mK Jy^{-1} sr^{-1} and 1040 ± 100 mK, respectively. We find no systematic variation of slope with galactic longitude. Converting the radio brightness temperatures to intensities in Jy sr^{-1}, the 60-μm to 11-cm and 60-μm to 6-cm intensity ratios are 700 and 810, respectively.

There are seven areas between 41° and 359° in galactic longitude for which the 6- and 11-cm surveys overlap. Hence, for each of these areas, a value for the 11- to 6-cm thermal spectral index can be calculated from the slopes of the lower envelopes. The average spectral index, α, where the brightness temperature $T_b(\nu) \propto \nu^{-\alpha}$ is 2.2 ± 0.4 compared with 2.1 predicted theoretically by the thermal bremsstrahlung mechanism. This gives some support to our method of fitting the lower envelopes.

All of these figures were derived following subtraction of the 'standard grain' variant of the H I-associated component. The effect of the subtraction of the alternative 'small grain' prediction of the H I-associated emission at 60 μm on the radio thermal–non-thermal separation was studied for a restricted area of the galactic plane from longitude 11°–53° and $|b| \leqslant 1.5°$. We again took $6° \times 3°$ areas and plotted 11-cm brightness temperature against residual 60-μm intensity, and determined the lower envelope of each plot. The mean gradient of these seven lower envelopes is 4.7 ± 1.2 mK (MJy sr^{-1})$^{-1}$, a reduction of 27 per cent on the previous value. This change corresponds to about one standard deviation on the mean gradient of the lower envelope.

3.3 THE INFRARED EXCESS

From our determination of the constant ratio between the 60-μm emission due to dust associated with H II regions and the 11-cm emission, one may obtain a value of the infrared excess (IRE), defined in Section 2.5 as the ratio between the total infrared luminosity and the power input into Ly α photons. Since the 11-cm and *IRAS* surveys are of very similar angular resolution, we can equate the ratios of the intensities to the ratios of the fluxes. In order to calculate the fraction of the total IR flux emitted in the 60-μm band, we assume that the emission is due to dust grains within the H II region which have a temperature of 30 K and follow a λ^{-2} emissivity law. Taking an electron temperature of 7000 K and the ratio of IR to radio intensities from Section 3.2, we obtain a value for the IRE of 4 ± 2 for the 'standard grain' variant or 3 ± 1.5 for the 'small grain' variant. The error quoted here is our estimate taking into account both the scatter in the slopes of the lower envelopes for the different areas, and the possible range of temperature and emissivity law for the grains.

These values of the IRE are in accord with the value Mezger (1978) considered reasonable on theoretical grounds for the ELD H II region. It is, however, only about half of the value he obtained using the IR intensities of Low *et al.* (1977) and the diffuse free–free continuum emission at 1390 MHz deduced from the Westerhout (1958) and Mathewson, Healey & Rome (1962) thermal–non-thermal separations of the galactic emission. Sodroski *et al.* (1987) found a mean value of 7 for the IRE of emission from the galactic plane. In both of these works, no subtraction of the H I-associated emission from the total IR intensities had been performed and thus larger values for the IRE might be expected. The original definition of IRE applies only to compact H II regions and the ELD ionized regions in which the O stars are situated, rather than to a combination of these regions with regions of neutral gas whose associated dust is heated mainly by the general ISRF and which presumably are exposed to fewer Ly α photons. Myers *et al.* (1986) calculated a median value of 6 for the IRE of 25 far-IR sources which had associated H II regions. Unlike Gispert, Puget & Sera (1982), Myers *et al.* found no evidence for a longitude dependence of the IRE. This observation supports our use of a constant value for the ratio between 60-μm and radio continuum emission, although on smaller scales the IRE probably does vary.

4 Separation of the thermal and non-thermal radio emission

With the relationship between the thermal radio continuum emission and the net 60-μm IR emission empirically determined, one can use this IR emission to identify and subtract off the thermal component of the radio emission from the observed total radio emission pixel by pixel. The 11-cm survey in its present form does not contain an accurate representation of the larger-scale structure of the non-thermal emission, so that the resultant maps primarily show the discrete non-thermal sources. Most of these are catalogued supernova remnants (SNR) but we have been able to identify a number of uncatalogued SNR candidates from the 11-cm survey. As was mentioned in Section 1, Fürst *et al.* (1987) have developed independently a similar procedure based on the ratio of IR to radio emission for identifying discrete non-thermal galactic sources which they are applying to the 11-cm survey. We shall therefore discuss this survey no further here but turn to the 6-cm survey instead.

4.1 SUPERNOVA REMNANT CANDIDATES FROM THE PARKES 6-cm SURVEY

The derived thermal component of the 6-cm radio emission has been subtracted pixel by pixel from the total 6-cm emission for all latitudes included in the survey over a longitude range $40° \geqslant l \geqslant 278°$. Comparison with the same area at 60 μm has enabled us to pick out objects which we consider as predominantly non-thermal sources but which are not known to be SNRs. A list of these sources is given in the Appendix, with their total 6-cm flux densities. The flux from the same area in the 60-μm band gives the 60-μm to 6-cm flux ratio listed in column 3. All of the objects have 6-cm flux densities $\geqslant 0.2$ Jy and a 60-μm to 6-cm flux ratio < 120. By comparison, the ratio for extended H II regions as derived from the lower envelope of the scatter plots is 800 and that of compact H II regions is > 500.

Of the 44 sources listed, 25 are unresolved (i.e. they have a diameter < 4 arcmin). The number counts of radio galaxies at 5 GHz (Wall & Cooke 1975) indicate that there should be approximately 48 extragalactic radio sources over the 524 square degrees of the survey with flux densities > 0.3 Jy. Some fraction of those that lie in bright regions close to the galactic plane are liable to be missed, however. The flux-angular size distribution of radiogalaxies of Swarup & Subrahmanya (1976) suggests that approximately four should be resolved by the 4.4-arcmin beam. These estimates are consistent with all of the unresolved sources in the table being radiogalaxies.

4.2 THERMAL AND NON-THERMAL COMPONENTS AT 408 MHz

We have applied the thermal–non-thermal separation technique to the area within 8° of the galactic plane of the 408-MHz all-sky map of Haslam *et al.* (1982). The zodiacal light and the H I-associated emission were removed from all 12 of the 60-μm galactic plane maps of the *IRAS* survey. The empirical scaling factor between the 60-μm and 11-cm intensities obtained in Section 3 was applied to give the distribution of thermal emission at 11 cm. This was then scaled to 408 MHz using a thermal spectral index of 2.1. Finally these data were convolved to the 51 arcmin resolution of the 408-MHz survey. The spectral index of 2.1 applies provided that the emitting regions are optically thin down to 408 MHz. This is true everywhere except for a few very bright H II regions. Shaver & Goss (1970) give directly measured flux densities at 408 MHz for these sources. Where these fluxes are less than those derived from the IR emission, the observed flux has been used.

The resulting distribution of thermal emission at 408 MHz for $|l|<90°$ is shown as the central maps in Figs 10 and 11. This component can then be subtracted from the total emission (upper maps) to give the distribution of non-thermal emission (lower maps). As we are interested in the larger-scale distribution of this emission, we have also subtracted from the lower maps the contributions from all catalogued SNR within 2° of the galactic plane which are unresolved at 51 arcmin.

The same data are presented as cuts along $b=0°$ in Fig. 12. Interpretation of these results in terms of the distribution of cosmic ray electrons and magnetic field will be given in a future publication. We note here that the relationship derived from the inner part of the galactic disc between the infrared and thermal radio emission appears to apply well to the relatively nearby Cygnus X complex. A more detailed study of the thermal–non-thermal separation of this region using the 11-cm survey by Wendker (1970) would be worthwhile. The peak at $l=8°$ in the galactic plane profile of Fig. 12 is due to the SNR candidate 8.7 – 0.2 listed in the Appendix. This appears to be a definite bright SNR. Its identification may have been hampered by an H II region which covers part of its area.

The results in Figs 10, 11 and 12 were obtained using the 'standard grain' variant of the H I-associated emission. Fig. 13 shows the sensitivity of the deduced thermal component to the grain model used in predicting the H I-associated IR emission. The 'small grain' variant results in a somewhat smaller thermal component. Because the non-thermal component dominates at 408 MHz, the relative uncertainty in this separated component, due to uncertainties in the grain model, amount to no more than about 7 per cent.

5 Discussion

5.1 THERMAL–NON-THERMAL SEPARATION

It is instructive to compare the results of this new method of separating the thermal and non-thermal components of the radio continuum emission of the Galaxy with the results of the spectral index technique. Mezger (1978) gives a peak brightness temperature profile along the galactic plane of thermal emission from the diffuse ionized gas at 1390 MHz, which is an average of two distributions from Westerhout (1958) and Mathewson *et al.* (1962). We can obtain a similar profile by scaling from our 408-MHz thermal component using a brightness temperature spectral index of 2.1. By drawing a lower envelope through the minima in the profile, we can directly compare the temperatures derived by the two approaches. We find that our deduced thermal emission is consistently lower, having brightness temperatures only 25–50 per cent of those given by Mezger. This suggests that either we have missed some of the

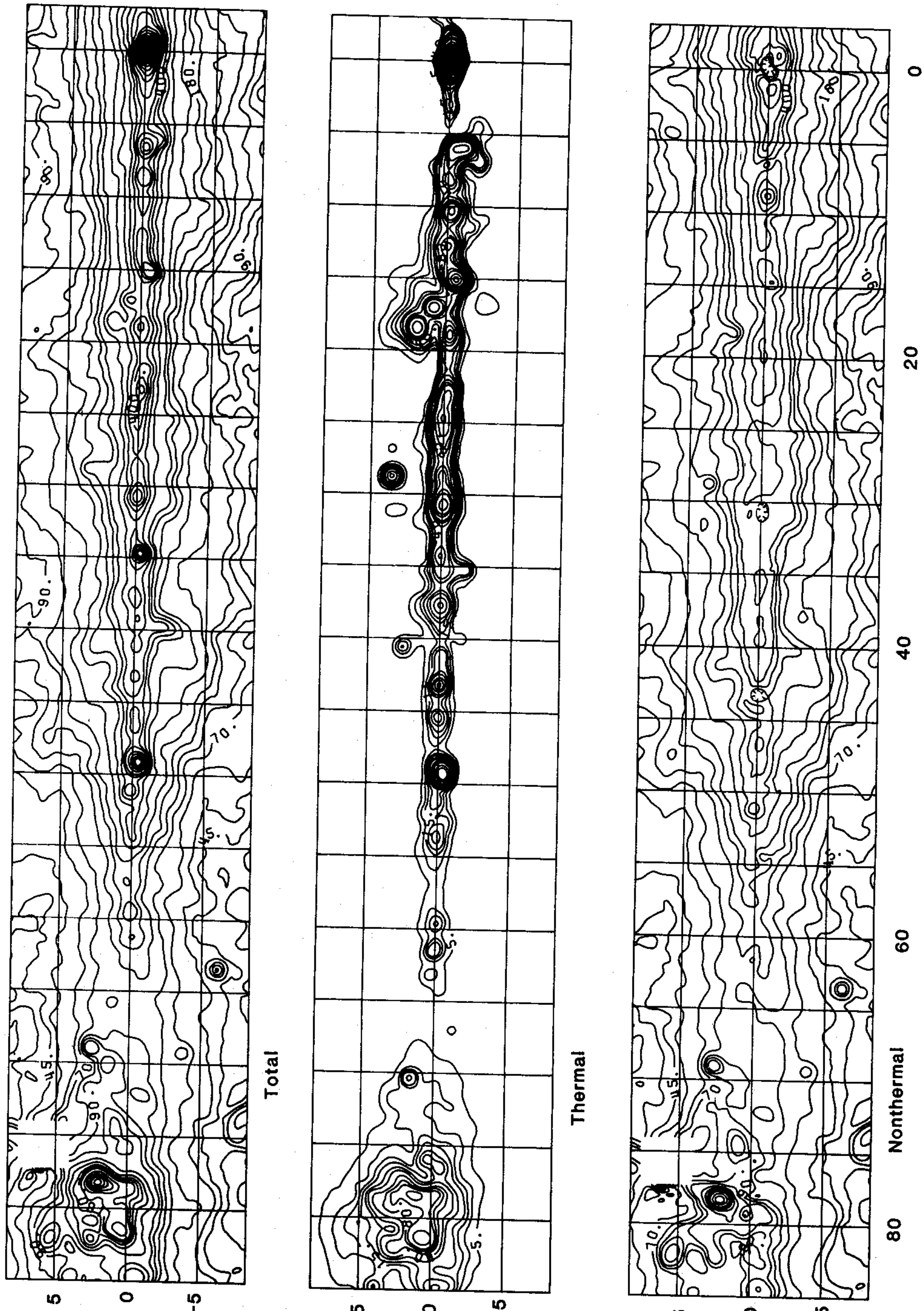

Figure 10. Contour maps of the 408-MHz emission from the galactic disc in the first quadrant of galactic longitude showing thermal–non-thermal separation. Upper map: the total brightness temperatures observed by Haslam *et al.* (1982). Middle map: the thermal component deduced from the 60-μm band *IRAS* data as detailed in the text. Bottom map: the non-thermal (synchrotron) component with known supernova remnants removed. Contour levels for the total and non-thermal maps are from 20 K, by 5–50 K, by 10–100 K, by 20–200 K, by 50–400 K and then by 100 K. Contour levels for the thermal map are from 5 K by 5–20 K, by 10–60 K, by 20–100 K, by 40–200 K, and then by 100 K.

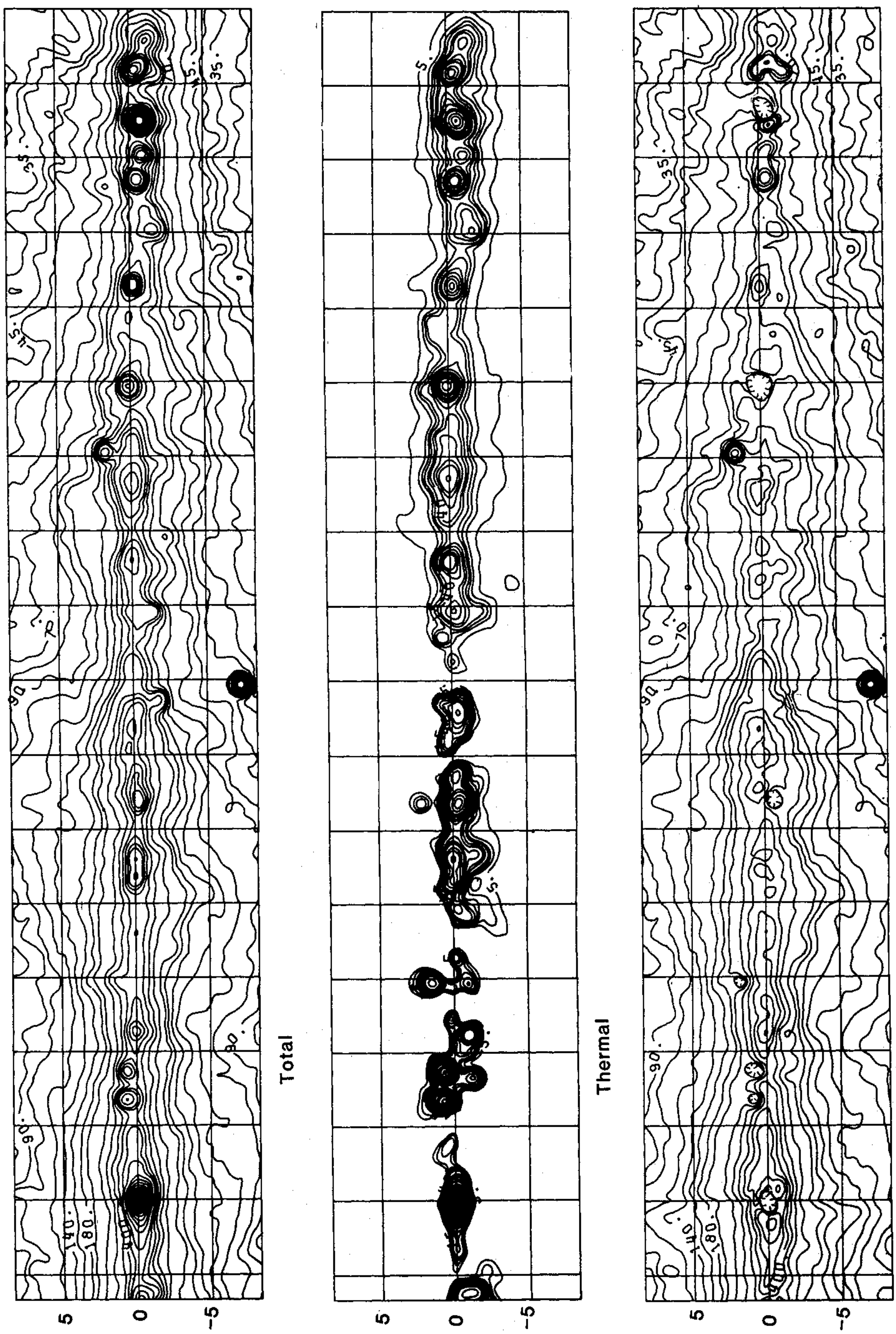

Figure 11. As for Fig. 10 but for the fourth quadrant of galactic longitudes.

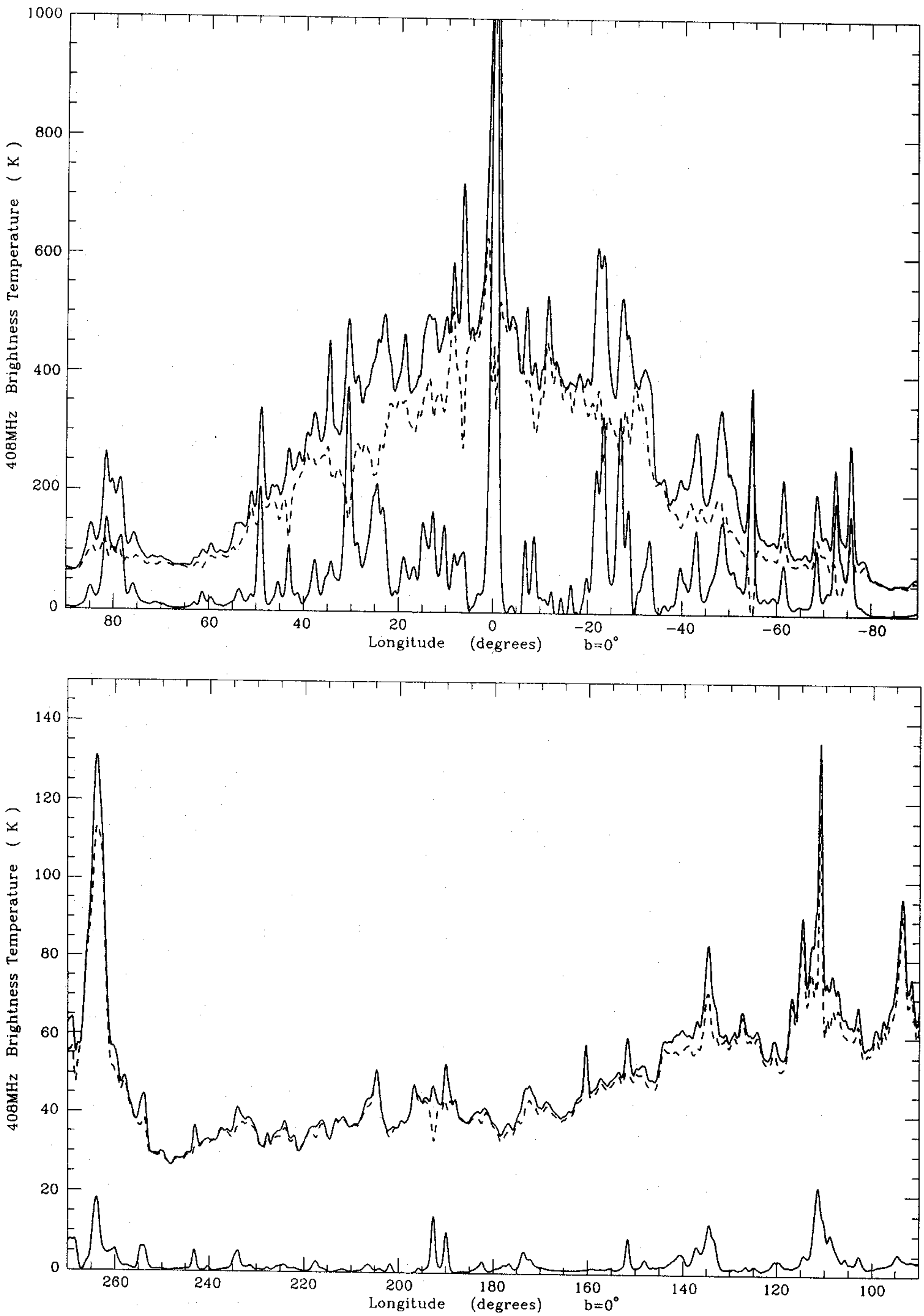

Figure 12. Cuts along $b = 0°$ of the 408-MHz emission with thermal–non-thermal separation. Top solid curve: total emission. Dashed curve: non-thermal emission. Lower solid curve: thermal emission.

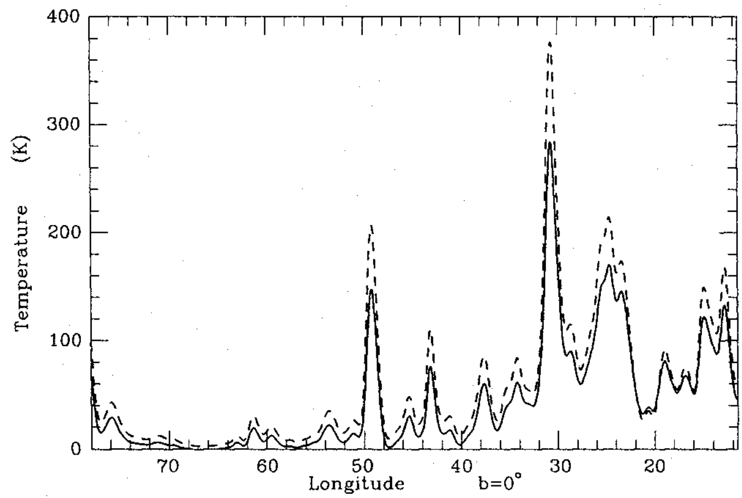

Figure 13. Cut along $b = 0°$ of the 408-MHz thermal emission derived using the 'standard grain' model of the H I-associated emission (dashed line) and the 'small grain' model (solid line).

thermal emission or that the spectral index technique has in this case overestimated the thermal emission.

Although, from the simple derivation of the infrared excess outlined in Section 2.5, the total IR emission should scale with the thermal radio continuum regardless of the density of the gas, one would, perhaps, expect the scaling to break down when one considers the IR emission in a specific waveband. The temperature of the dust could be lower near to the edges of the extended low-density regions than near their centres. This would mean that the fraction of the total IR emission falling in the 60-μm band would be smaller near the edges. Assuming a λ^{-2} emissivity law for the dust grains, the fraction of the total IR emission in the 60-μm band from dust at 20 K is only about 28 per cent of that at 30 K. It would seem from this argument that it would have been better to correlate the radio emission with the total IR emission estimated from a consideration of the relative and absolute intensities in the 60- and 100-μm bands. It can be seen from the almost constant ratio of the two observed intensities, however, that this procedure would have made little difference. There seems to be no direct evidence from a comparison of the 60- and 100-μm band observations for lower temperatures near the edges of the ELD H II regions, although the postulated small grains, possible line emission and the effect of averaging along the line-of-sight might conspire to mask it.

As an illustration of some of the problems of the spectral index method for thermal–non-thermal separation, we consider some of the details of its application to the survey of Westerhout. This was made at 1390 MHz with a beam size of 34 arcmin. The low-frequency survey with which it was compared was that of Hill, Slee & Mills (1958), made with the Mills cross at 85.5 MHz. In principle, the zero levels and temperature scales of the two surveys have to be known for this method to work. The low-frequency brightness temperatures were assumed to have been absolutely determined, but the 1390-MHz brightness temperatures had been measured with respect to an unknown zero level. In the original paper an estimate of this level was made via that of an earlier survey at 900 MHz. It was checked by assuming that at the limits of the 85.5-MHz survey ($b = \pm 5°$) the emission would be entirely non-thermal, and by extrapolating the brightness temperatures at these limits to 1390 MHz using a non-thermal spectral index of 2.7. This index was the mean of a number of earlier high-latitude measurements over a range of frequencies. The check showed an inconsistency which could be resolved if the 1390-MHz temperature scale were multiplied by 0.75 or the 85.5-MHz temperature scale were multiplied by 1.32. It was decided to leave the temperature scales unchanged and to use instead a non-thermal spectral index of 2.6. The thermal emission plotted by Mezger (1978) follows a reworking of the Westerhout data. Observation of Cas A had shown that the 1390-MHz temperature scale needed to be multiplied by a correction factor of 0.81. The zero level was determined from the temperatures at the edges of the 85.5-MHz survey using a non-thermal spectral index of 2.7 as above.

The validity of these corrections to the scales and the fixing of the zero levels of the Westerhout and Mathewson surveys can be checked by comparing them with the Stockert 1420-MHz northern sky survey (Reich 1982; Reich & Reich 1986) made with a similar angular resolution. For three points along the galactic plane, where Westerhout's lower envelope of the 1390-MHz profile corresponds to the total brightness temperature, we calculated what the corresponding temperatures would be from the Stockert survey by subtracting a 2.8-K extragalactic background and scaling from 1420 to 1390 MHz. The comparison is given in Table 1.

Table 1. Brightness temperature (K).

l (°)	Westerhout	Mathewson *et al.*	Stockert
38.8	10.9	10.5	8.5
36.3	12.0	12.0	8.7
24.8	18.7	17.2	16.6

It can be seen that both the Westerhout and Mathewson *et al.* temperatures are significantly higher than the carefully calibrated full-beam temperatures of the Stockert suvey. Assuming that the more recent survey is correct, the spectrum of total emission deduced earlier is too flat, and the fraction of the emission deduced to be thermal is too high. The discrepancies between the three surveys most likely arose in the determination of the absolute temperature and scale. These can be a major source of uncertainty in applying the spectral index technique.

Reich & Reich (1988) have determined the spectral index of the total emission between the Haslam *et al.* survey at 408 MHz and the Stockert survey at 1420 MHz after the latter had been convolved to the 51 arcmin resolution of the former. They have performed a thermal–non-thermal separation over the longitude interval $50° \geqslant l \geqslant 10°$. In this interval along the galactic plane, the spectral index of the total emission is everywhere > 2.6, so that if the non-thermal spectral index of Westerhout had been adopted there would have been no thermal component at all. The authors argued, however, mainly from earlier observations at frequencies between 1.4 and 15.5 GHz that the spectral index of the non-thermal emission should be 3.1. The thermal component which they deduced using this is generally at the same level as that deduced by us, with our estimates having larger excursions from the mean. This would imply, if our separation is correct, that the non-thermal emission does indeed have a rather steep spectrum between 408 and 1420 MHz but that its spectral index varies somewhat from one longitude to the next in the inner Galaxy.

The assumptions of a non-thermal spectral index of 2.6 between 85.5 and 1390 MHz by Westerhout and of a non-thermal spectral index of 3.1 between 408 and 1420 MHz by Reich & Reich are not obviously incompatible. One might argue that the non-thermal spectrum steepens quite sharply at about 408 MHz and that its spectral index is much less than 2.6 between 85.5 and 408 MHz. What is difficult to accept, bearing in mind that the strength of the galactic magnetic field is expected to increase towards the centre of the Galaxy, is that the steepening in the spectrum occurs at the same frequency at all points along the line-of-sight.

5.2 LUMINOSITY OF THE GALAXY AT 60 μm

We have attempted to construct a picture of the galactic radial distribution of the H II-associated 60-μm band emission by using the unfolding procedure of Strong (1975). It is assumed that there is cylindrical symmetry about the galactic centre for the north and south sides of the Galaxy separately. The H II regions are assumed to be in a disc of total thickness $260r$ pc and radius $10r$ kpc, i.e. there is no appreciable emission outside the solar circle. Here we express deduced quantities in terms of $r = R_0/10$ where R_0 is the distance of the Sun from the Galactic Centre in kpc. These simplifying assumptions are somewhat crude but should allow the determination of the radial distribution of emission with sufficient accuracy to allow the conversion of the directly observed line-of-sight column intensities to total flux for the Galaxy as a whole.

Line intensities were obtained from our estimation of the contribution to the 60-μm band emission from H II regions within 1°.5 of the galactic plane. The unfolding was performed on the north and south sides of the inner Galaxy separately and an estimation of the radial distribution of emissivity was made for each as shown in Fig. 14. The negative values indicate a breakdown in the assumed cylindrical symmetry. An asymmetry between the north and south sides is also apparent but both sides have a peak at about $5r$ kpc. The total luminosity deduced from this radial distribution is $1.6 \times 10^{23}\ r^2$ W Hz^{-1}. Of this, $1.2 \times 10^{23}\ r^2$ W Hz^{-1} originates further than r kpc from the Galactic Centre.

An estimate of the luminosity outside the solar circle was made by assuming that all of the H II-associated emission between $l = 76°$ and $l = 282°$ with $|b| < 1°.5$ is emitted uniformly over a volume between $10r$ and $13r$ kpc from the Galactic Centre. From this we conclude that the luminosity outside the solar circle is about $1.1 \times 10^{22}\ r^2$ W Hz^{-1}, which is only a small fraction of that within the solar circle.

For a comparison of these luminosities with the H I-associated luminosity of the Galaxy we refer to Li, Riley & Wolfendale (1983). Presented there is a plot of the surface density of neutral hydrogen as a function of galactocentric radius, which, together with the variation of

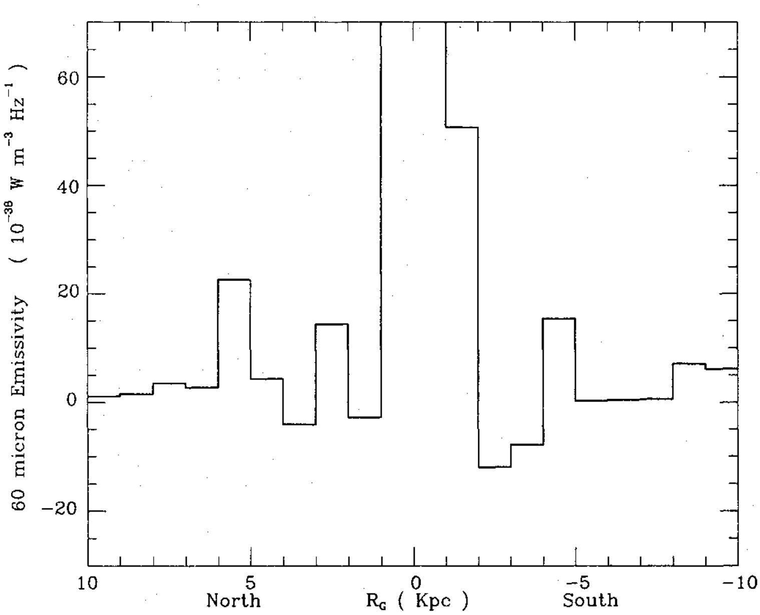

Figure 14. The distribution with galactocentric radius of the H II-associated 60-μm emissivity. The unfolding assumes azimuthal symmetry but the presence of some negative emissivities indicate that this is only approximately true. The north and south sides of the Galaxy are treated separately.

Table 2.

Component	Luminosity/W Hz^{-1} in *IRAS* 60-μm band	
	Inside solar circle ($r<R<10r$ kpc)	Outside solar circle ($R>10r$ kpc)
H I-associated	$1.5\times10^{23}\,r^2$	$10^{22}\,r^2$
H II-associated	$1.1\times10^{23}\,r^2$	$10^{22}\,r^2$

dust emissivity per H atom (see Section 2.3), can be used to calculate the total luminosity in the 60-μm band of H I-associated dust in the galactic disc. The results are summarized in Table 2.

Thus we deduce that, in the inner Galaxy, about 58 per cent of the 60-μm band emission is H I-associated and 42 per cent is H II-associated.

5.3 MASS OF IONIZED GAS

Another quantity which we can estimate from our deduced thermal component of the radio continuum emission is the total mass of ionized gas in the Galaxy. We use the above radial distribution of 60-μm emissivity scaled by 1.4×10^{-3} to give the thermal radio emissivity at 11 cm. Assuming that this emission is due to thermal bremsstrahlung one can derive an rms electron density for each 1 kpc wide annulus about the Galactic Centre. This value must be multiplied by the square root of the clumping factor, K, in order to obtain the actual density. The unfolding could extend only to $10r$ kpc. An estimate of the, small, electron density outside the solar circle was made by assuming that all of the 60-μm emission observed outside the longitude range used for the unfolding (i.e. $282°\geqslant l\geqslant 76°$) emanates from a circular annulus of internal and external radii $10r$ and $13r$ kpc respectively. To calculate the total mass of ionized hydrogen in the Galaxy, excluding the central 1 kpc, we assume a constant scale height $130r$ pc. Multiplying the derived H mass by 1.4 to include ionized He we obtain the total mass of ionized gas

$$M_{ion}=9.9\times10^{8}\,K^{-0.5}\,r^2\,M_\odot \qquad \text{for } R\geqslant r \text{ kpc.}$$

This is a rather crude estimate, since the assumption of cylindrical symmetry about the Galactic Centre is undoubtedly an over-simplification. A more refined approach would be to consider the spiral structure of the Galaxy. Mezger (1978) deduced from his assumed diffuse free–free continuum galactic flux a total mass of ionized gas between $0.8r$ and $10r$ kpc of $1.0\times10^{9}\,K^{-0.5}\,r^2\,M_\odot$, while our estimate for the same region is $7.8\times10^{8}\,K^{-0.5}\,r^2\,M_\odot$.

5.4 THERMAL AND NON-THERMAL RADIO LUMINOSITY OF THE GALAXY

The thermal part of the total radio continuum luminosity of the Galaxy can be calculated in a similar way to that described in Section 5.2. At 408 MHz the thermal luminosity is 2.1×10^{20} r^2 W Hz^{-1}, while at 5 GHz it is 1.6×10^{20} r^2 W Hz^{-1}. As can be seen in Fig. 10, the non-thermal component has a much wider distribution of intensity about the galactic plane than the thermal component, and a more complex model of the three-dimensional distribution of emissivity is required. Phillipps *et al.* (1981), from a detailed consideration of the distribution of 408-MHz intensity over the whole sky, derived a model having a 'thick disc' with width ~1 kpc and a lower emissivity non-spherical 'halo' extending to ~10 kpc from the plane. By integrating this emissivity distribution, a non-thermal luminosity at 408 MHz of $8.5 \times 10^{21}\ r^2$ W Hz^{-1} is obtained. Thus the ratio of thermal to non-thermal luminosity at 408 MHz is 2.5 per cent. It is more difficult to determine the non-thermal luminosity at 5 GHz. The brightness temperature at $|b| > 2^\circ\!.5$ would be expected to be < 0.1 K and cannot be measured absolutely. Nevertheless its distribution across the sky is needed in order to obtain the total luminosity. If one takes the 5-GHz distribution as following that at 408 MHz, one is assuming a uniform spectral index throughout the Galaxy. Close to the galactic plane in the inner parts of the Galaxy, the thermal–non-thermal separation indicates a spectral index ~ 0.7 between 408 MHz and 5 GHz for the non-thermal component. There are independent indications, however, that the radio spectrum is steeper at higher galactic latitudes and in the outer parts of the Galaxy, and an effective index over the whole sky may be as large as 1.0. Using these values as limits, the non-thermal luminosity at 408 MHz scales to $(11 \pm 4) \times 10^{20}\ r^2$ W Hz^{-1} at 5 GHz and the ratio of thermal to non-thermal luminosity is 15 ± 5 per cent.

Duric, Bourneuf & Gregory (1988) have applied the spectral index technique to thermal–non-thermal separation of the flux from a selection of spiral galaxies. The spectral index of the thermal component is taken to be 0.1, while that of the non-thermal component is a free parameter but is assumed to be constant from 0.1 to 10 GHz. For those galaxies to which such model spectra can be fitted, there is a rather wide range of thermal fractions at 5 GHz. The above value for the Galaxy is typical of those for galaxies of similar luminosity class.

A number of authors have pointed out the tight correlation between the far-infrared and radio continuum luminosities of spiral galaxies. Hummel *et al.* (1988) have made a detailed study of the correlations between these and the optical and neutral hydrogen properties of 88 Sbc galaxies. The mean ratio between the radio luminosity at 1.5 GHz and the infrared luminosity at 100 μm is 2.0×10^{-3}. We deduce that the corresponding value for the Galaxy is $(2.1 \pm 0.4) \times 10^{-3}$, where the uncertainty is due to the spectral index used in scaling the non-thermal component from 408 MHz. The radio emission at 1.5 GHz from all of these galaxies will be predominantly non-thermal, and the inference which has been drawn is that the cosmic ray content of the galaxies is closely related to the recent star-formation rate as measured by the H II-associated infrared emission. (The probable lifetime of cosmic rays in the galaxies and the ages of the stars producing the H II regions are both of the order of 10^7 yr.) The tightness of the correlation is rather suprising, however, in view of the fact that the radio emission depends on the galactic magnetic field strength as well as the cosmic ray content and that about half of the infrared emission is from dust in H I regions which are associated with an older population of stars. It seems that there may be a link between the recent star-formation rate and the magnetic field, although in which direction this operates is not clear. The level of H I-associated emission depends on the ISRF and may be influenced in the inner parts of the galaxies by the recent star-formation rate. It is important to note that this tight correlation is between the global emission from the galaxies and not between the distributions within galaxies. In those galaxies, including our own, where the distribution of non-thermal emission about the galactic plane is known, it is wider by about an order of magnitude than the distribution of infrared emission. Only a small part of the total non-thermal emission comes from the gaseous disc of the Galaxy where the infrared emission is concentrated.

6 Conclusions

Our main conclusion is that there is a component of the far-infrared radiation from the galactic disc, strong in the 60-μm *IRAS* band, which correlates so well with the short-wavelength radio continuum emission that it must originate in regions of ionized hydrogen. This includes extended low-density H II regions as well as discrete sources. The corollary of this is that the 60-μm band emission, after due allowance has been made for the H I-associated emission, can be used to identify the thermal component of the radio continuum. On a small scale this can be used to distinguish non-thermal sources (supernova remnants and radio galaxies) from H II regions. A list of supernova remnant candidates has been produced for the southern hemisphere. On a larger scale, the technique has been used to remove the thermal contribution from the 408-MHz all-sky map by Haslam *et al.* (1982). The more detailed picture of the distribution of synchrotron radiation near to the galactic plane that this reveals will be dealt with in a future paper.

The apparent colour temperature of the total infrared emission, based on the *IRAS* 60- to 100-μm band intensity ratio does not agree with that expected if the emission is solely from graphite and silicate grains in radiative equilibrium with their local ISRF. As an alternative to an explanation in terms of a component of emission from smaller grains, not in radiative equilibrium, we suggest that, in the galactic plane in the inner part of the Galaxy, there may be a significant contribution to the 100-μm band from O III line emission from H II regions. This would also be expected to correlate with the thermal radio continuum and could account for an apparent decrease in colour temperature of the H II-associated emission with decreasing galactocentric radius. It is likely that the observed colour temperature is, in fact, due to a combination of the two effects. These alternatives have a bearing on our procedure for thermal–non-thermal separation of the radio continuum via their effect on the predicted H I-associated component. In order to quantify this, we have performed the separation both for the model of 'standard grains' plus line emission and for the 'small grain' model.

The thermal component which we have deduced at 408 MHz is somewhat smaller than inferred from the early spectral index separation of Westerhout (1958), but is at about the same level as that deduced more recently by Reich & Reich (1988). The disagreement between the two distributions derived using the spectral index technique illustrates the problems of applying it. By embarking on a programme to develop a new procedure using the *IRAS* 60-μm band emission, as described in the present work, we hope to circumvent such difficulties.

Acknowledgments

The authors value the discussions they have had with P. Cox, P. G. Mezger and A. W. Wolfendale. The IPMAF team at the Rutherford Appleton Laboratory are thanked for providing the *IRAS* data and software. AB acknowledges SERC for her Research Studentship.

References

Altenhoff, W. J., Downes, D., Goad, L., Maxwell, A. & Rinehart, R., 1970. *Astr. Astrophys. Suppl.*, **1**, 319.
Boulanger, F. & Pérault, M., 1988. *Astrophys. J.*, **330**, 964.
Broadbent, A., Osborne, J. L. & Haslam, C. G. T., 1988. In: *Comets to Cosmology, 3rd IRAS Symp.*, p. 109, ed. Lawrence, A., Springer-Verlag, Berlin.
Burton, W. B. & Gordon, M. A., 1978. *Astr. Astrophys.*, **63**, 7.
Burton, W. B., Deul, E. R., Walker, H. J. & Jongeneelen, A. W. W., 1986. In: *Light on Dark Matter*, ed. Israel, F. F., Reidel, Dordrecht.
Cox, P., Krügel, E. & Mezger, P. G., 1986. *Astr. Astrophys.*, **155**, 380.
Draine, B. T. & Anderson, N., 1985. *Astrophys. J.*, **292**, 494.
Draine, B. T. & Lee, H. M., 1984. *Astrophys. J.*, **285**, 89.

Duric, N., Bourneuf, E. & Gregory, P. C., 1988. *Astr. J.*, **96**, 81.
Fürst, E., Reich, W. & Sofue, Y., 1987. *Astr. Astrophys. Suppl.*, **71**, 63.
Gispert, R., Puget, J.-L. & Sera, G., 1982. *Astr. Astrophys.*, **106**, 293.
Güsten, R. & Mezger, P. G., 1983. *Vistas Astr.*, **26**, 159.
Harwit, M., Houck, J. R. & Stacey, G. J., 1986. *Nature*, **319**, 646.
Haslam, C. G. T. & Osborne, J. L., 1987. *Nature*, **327**, 211.
Haslam, C. G. T., Salter, C. J., Stoffel, H. & Wilson, W. E., 1982. *Astr. Astrophys. Suppl.*, **20**, 37.
Haynes, R. F., Caswell, J. L. & Simons, L. W. J., 1978. *Aust. J. Phys. Astrophys. Suppl.*, **45**, 1–87.
Heiles, C. & Cleary, M. N., 1979. *Aust. J. Phys. Astrophys. Suppl.*, **47**, 1.
Heiles, C. & Habing, H. J., 1974. *Astr. Astrophys. Suppl.*, **14**, 1.
Hill, E. R., Slee, O. B. & Mills, B. Y., 1958. *Aust. J. Phys.*, **11**, 530.
Hummel, E., Davies, R. D., Wolstencroft, R. D., van der Hulst, J. M. & Pedlar, A., 1988. *Astr. Astrophys.*, **199**, 91.
IRAS Explanatory Supplement, 1985. Eds Beichman, C. A., Neugebauer, G., Habing, H. J., Clegg, P. E. & Chester, T. J., JPL D-1855, Jet Propulsion Laboratory, Pasadena.
Li, Ti Pei, Riley, R. A. & Wolfendale, A. W., 1983. *Mon. Not. R. astr. Soc.*, **203**, 87.
Low, F. J., Kurtz, R. F., Pateet, W. M. & Nishimura, T., 1977. *Astrophys. J.*, **214**, L115.
Low, F. J. *et al.*, 1984. *Astrophys. J.*, **278**, L19.
Mathewson, D. S., Healey, J. R. & Rome, J. M., 1962. *Aust. J. Phys.*, **15**, 354 and 369.
Mathis, J. S., Rumpl, W. & Nordsieck, K. H., 1977. *Astrophys. J.*, **217**, 425.
Mathis, J. S., Mezger, P. G. & Panagia, N., 1983. *Astr. Astrophys.*, **128**, 212.
Mezger, P. G., 1978. *Astr. Astrophys.*, **70**, 565.
Mezger, P. G., Mathis, J. S. & Panagia, N., 1982. *Astr. Astrophys.*, **105**, 372.
Myers, P. C., Dame, T. M., Thaddeus, P., Cohen, R. S., Silverberg, R. F., Dwek, E. & Hauser, M. G., 1986. *Astrophys. J.*, **301**, 398.
Phillipps, S., Kearsey, S., Osborne, J. L., Haslam, C. G. T. & Stoffel, H., 1981. *Astr. Astrophys.*, **103**, 405.
Reich, W., 1982. *Astr. Astrophys. Suppl.*, **48**, 219.
Reich, P. & Reich, W., 1986. *Astr. Astrophys. Suppl.*, **63**, 205.
Reich, P. & Reich, W., 1988. *Astr. Astrophys.*, **196**, 211.
Reich, W., Fürst, E., Steffen, P., Reif, K. & Haslam, C. G. T., 1984. *Astr. Astrophys. Suppl.*, **58**, 197.
Sanders, D. B., Clemens, D. P., Scoville, N. C. & Solomon, P. M., 1986. *Astrophys. J. Suppl.*, **60**, 1.
Shaver, P. G. & Goss, W. M., 1970. *Aust. J. Phys. Astrophys. Suppl.*, **14**, 133.
Sodroski, T. J., Dwek, E., Hauser, M. G. & Kerr, F. J., 1987. *Astrophys. J.*, **322**, 101.
Strong, A. W., 1975. *J. Phys. A*, **8**, 617.
Strong, A. W., Riley, P. A., Osborne, J. L. & Murray, J. D., 1982. *Mon. Not. R. astr. Soc.*, **201**, 495.
Swarup, G. & Subrahmanya, C. R., 1976. *Radioastronomy and Cosmology, IAU Symp. No. 74*, p. 125, ed. Jauncey, D. L., Reidel, Dordrecht.
Terebey, S. & Fich, M., 1986. *Astrophys. J.*, **309**, L73.
Wall, J. V. & Cooke, D. J., 1975. *Mon. Not. R. astr. Soc.*, **171**, 9.
Watson, D. M., Storey, J. W. V., Townes, C. H. & Haller, E. E., 1981. *Astrophys. J.*, **250**, 605.
Weaver, H. & Williams, D. R. W., 1973. *Astrophys. Suppl.*, **8**, 1.
Wendker, H. J., 1970. *Astr. Astrophys.*, **4**, 378.
Westerhout, G., 1958. *Bull. astr. Inst. Neth.*, **14**, 215.

Appendix

Table A1 gives a list of non-thermal radio sources picked out from the 6-cm survey by Haynes *et al.* (1978) by their much lower ratio of 60-μm to 6-cm flux than is observed in H II regions. None of these has been catalogued as a supernova remnant. Two are known to be radio-galaxies. Statistically, all of those which are unresolved by the 4-arcmin beam could also be radiogalaxies. The remaining 17 are prime candidates for supernova remnants.

Table A1. Non-thermal sources including supernova remnant candidates.

Galactic Coordinates l	b	6 cm Flux Jy	60 μm/6 cm Flux Ratio	Comments
280.2	+1.5	0.3	0	unresolved
284.3	-1.6	9.1	0	
286.0	-1.1	2.1	0	unresolved
286.8	-0.0	12.0	0	
289.1	-2.8	1.1	0	unresolved
290.8	+0.8	1.4	23	unresolved
299.7	-1.4	0.2	26	unresolved
309.7	+1.7	57.0	2	radiogalaxy
312.9	-0.1	2.7	0	
313.6	+1.3	0.85	0	unresolved
314.0	+1.0	1.1	54	
318.9	-0.5	1.1	54	
319.0	+0.4	3.0	57	
321.5	+1.0	1.2	0	unresolved
322.1	+0.0	1.3	0	unresolved
322.1	+1.4	1.6	0	unresolved
325.5	+1.7	1.3	0	unresolved
339.5	-1.3	3.4	0	
341.8	+1.8	0.96	46	
347.7	-1.2	1.8	58	unresolved
357.2	-0.2	0.8	0	
2.9	-2.8	2.5	0	unresolved
3.7	+0.6	0.6	0	unresolved
5.3	-2.5	0.7	0	
5.6	+1.4	0.32	39	unresolved
6.3	+1.9	0.36	0	unresolved
6.6	+1.4	0.5	0	unresolved
8.7	-0.2	14.3	0	
9.7	-0.1	1.1	29	
15.4	+0.2	0.73	0	
15.5	-0.1	0.67	0	
16.7	+0.1	1.5	73	unresolved
19.3	+2.2	1.5	0	unresolved
21.0	+2.0	2.7	21	unresolved
21.3	-0.6	1.6	0	unresolved
24.9	-1.8	0.5	20	unresolved
28.8	-0.5	0.3	0	
29.4	+0.1	1.7	45	
30.1	+1.3	2.3	20	radiogalaxy
31.6	-0.6	1.4	0	
32.3	+1.2	0.38	111	unresolved
36.5	-0.0	0.47	0	unresolved
39.7	-2.2	0.47	8	unresolved
40.1	-2.3	0.4	5	unresolved